Geofísica Internacional (2014) 53-4: 435-456

Original paper

Ca. 13 Ma strike-slip deformation in coastal Sonora from a large-scale, *en-echelon*, brittle-ductile, dextral shear indicator: implications for the evolution of the California rift

David García-Martínez*, Roberto Stanley Molina Garza, Jaime Roldán Quintana, Hector Mendívil-Quijada

Received: September 02; 2013; accepted: February 18, 2014; published on line: October 01, 2014

Resumen

La estructura semicircular Rancho Nuevo es una estructura geomorfológica definida por patrones de drenaje en la planicie costera de Sonora, localizada a 160 kilómetros al noroeste de Hermosillo. Su extensión es de 15 por 30 kilómetros y está compuesta por un núcleo de plutones de composición félsica-intermedia (granodiorita, monzogranito, cuarzo pórfido y granito), cubiertos por rocas volcánicas del Mioceno. Este trabajo está enfocado a la deformación de los intrusivos que abarcan casi la totalidad del área de estudio. Los plutones consisten en una serie co-magmática fechada entre 71 ± 1.1 y 67.9 ± 1.0Ma (U-Pb en circones, LA-ICP-MS). La unidad más voluminosa es una granodiorita caracterizada por un fracturamiento conspicuo de forma sigmoidal visible a escala de imágenes de satélite de alta resolución, a lo largo del cual se emplazaron diques de composición riolítica de 13.2 Ma (U-Pb en circones, LA-ICP-MS). La fabrica magnética (AMS) y los datos paleomagnéticos fueron colectados en 27 sitios en la unidad granodiorita. La fábrica magnética es débil pero bien definida y se caracteriza por contener planos de foliación en la roca bien desarrollados con rumbos que siguen el patrón de fracturamiento sigmoidal sugiriendo un aplanamiento NE-SW a NW-SE, posterior al emplazamiento. La magnetización característica es de polaridad dual, pero dominantemente inversa y consistente con un emplazamiento durante el cron C31r. La magnetización prevalente es suroeste y moderadamente negativa (10 sitios), mostrando una rotación en sentido horario alrededor de 41º ± 11 con respecto a la dirección de referencia esperada del Cretácico Tardío. Sin embargo, existe evidencia paleomagnética que sugiere que la estructura Rancho Nuevo no rotó como un cuerpo rígido, sino que en su lugar se deformó internamente. Estos datos indican que la estructura semicircular Rancho Nuevo registra cizallamiento, dextral, frágil-dúctil, a gran escala. La edad de los diques y su relación discordante por rocas asignadas a la Toba San Felipe indican que el movimiento dextral de la península de Baja California (y por lo tanto la placa del Pacífico) afectó la costa de Sonora hace aproximadamente 13 Ma.

Palabras clave: Mioceno, Golfo de California, Sonora, rumbo de desplazamiento, paleomagnetismo

D. García-Martínez*
J. Roldán Quintana
H. Mendívil-Quijada
Posgrado en Ciencias de la Tierra
Universidad Nacional Autónoma de México
sede Hermosillo
Boulevard Colosio y Madrid, s/n
83000, Col. Centro
Hermosillo, Sonora, México
Corresponding author: davidgm1964@yahoo.com.mx

R. Stanley Molina Garza
Centro de Geociencias
Universidad Nacional Autónoma de México
Campus Juriquilla, 76230
Querétaro, México

Abstract

The Rancho Nuevo semi-circular structure is a geomorphological structure defined by drainage patterns in coastal Sonora, about 160 km NW of Hermosillo. The structure is about 15 by 30 km, and it is cored by felsic to intermediate plutons (granodiorite, monzogranite, quartz-porphyry) covered by Miocene volcanic rocks. This work is focused on the deformation of the intrusives which cover most of study area.The plutons are a co-magmatic suite dated between 71±1.1 and 67.9±1.0Ma (U-Pb zircon, LA-ICPMS). The most voluminous unit is a granodiorite characterized by conspicuous sigmoidal fractures at the scale of high resolution satellite images, along which rhyolite dikes were emplaced about 13.2 Ma. Magnetic fabric (AMS) and paleomagnetic data were collected from 27 sites in the granodiorite. Magnetic fabrics are weak but well developed, and are characterized by steep foliation planes with strikes that follow the sigmoidal fracture pattern and suggest NE-SW to NW-SE flattening after emplacement. The characteristic magnetization is of dual polarity, but it is dominantly reverse consistent with emplacement during chron C31r. The prevalent magnetization is southwest and moderately steep negative (ten sites), a discordant direction rotated clockwise about 41º±11 with respect to the expected Late Cretaceous reference direction, also indicating gentle southward tilt. There is, however, paleomagnetic evidence suggesting that the structure did not rotate as a rigid body, but it deformed internally instead. These data are interpreted to indicate that the Rancho Nuevo semicircular structure is a large-scale, dextral, brittle-ductile shear indicator. The age of the dikes and the fact that they are covered discordantly by rocks assigned to the tuff of San Felipe indicate that northwest, srike-slip, motion of Baja California peninsula (and thus the Pacific plate relative to North America) was accommodated by faults in coastal Sonora about 13 Ma ago.

Key words: Miocene, Gulf of California, Sonora, strike-slip, paleomagnetism

Introduction

Western North America is perhaps the best studied convergent margin in the world, and possibly the best suited to study oceanic plate-continent interactions. The arrival of the spreading center that existed between the Farallon and Pacific plates to the convergent margin of western North America by the end of Oligocene gave rise to major plate reorganization that subsequently resulted in deformation in the plate boundary region. The margin changed from subduction of the Farallon plate under North America to a dextral oblique transform between the Pacific plate and North America. This resulted, eventually, in rifting between Baja California and North America in the Miocene as this block was transferred to the Pacific plate. There is disagreement among the authors working in the region, however, on the timing and the geodynamics of the changes described above. One of the most contentious issues is whether the initial rifting process between Baja California and North America, between about 13 and 6 Ma, was orthogonal or dextral-oblique strike slip. Answering this question requires field studies, to determine the timing and kinematics of the faults along the plate boundary region.

Before the arrival of the Farallon-Pacific ridge to the continental margin, the plate boundary evolved as a compressional Cretaceous to Paleogene continental arc where subduction consumed the Farallon plate forming the Peninsular Ranges and the coastal Sonoran batholith.The semicircular structure Rancho Nuevo (RNSS) is part of the coastal Sonoran batholiths. This paper focus is on the deformation of the granitoids of the RNSS in the central coast of Sonora. New field work, geochronology, and paleomagnetic data show that Late Cretaceous intrusives were rotated about a vertical axis and deformed in a dextral-shear couple. This rotation and deformation of the RNSS are interpreted in terms of plate interactions, and contribute to better understanding the Gulf of California history. Here we interpret the semi-circular Rancho Nuevo structure as a feature produced by dextral shear *ca*. 13 Ma. The RNSS is a dextral, *en-echelon system*, with brittle-ductile structures associated to right-lateral faults that accommodated motion between Baja California (Pacific plate) and Sonora (North America plate).

Tectonic model for Cenozoic evolution of NW Mexico

The geologic evolution of NW Mexico is closely linked to oceanic plate-continent interactions. Subduction of the Farallon plate produced voluminous arc magmatism, and was also the main driver of the Late Cretaceous-Paleogene Laramide orogeny. The Laramide thickened the crust and created significant topography. This event was followed by the basin and range extensional episode along western North America; extension led to crustal thinning. Although the mechanisms for extension and

crustal thinning in the basin and range are under debate, these include gravitational collapse of over thickened crust, lithospheric delamination by a mantle plume, and plate boundary interactions such as a slow-down of the plate convergence rate.

The basin and range event is also associated with emplacement of large volumes of felsic and mafic volcanic products (bimodal volcanism). Damon *et al*. (1981) showed that the position of the magmatic front migrated eastward during the Laramide orogeny, from Sonora to central Coahuila, migrating back to the west during the basin and range extensional event to reach the longitude of the Gulf of California by mid-Miocene time. This evolution can be explained by subduction dynamics: flattening of the slab during the Laramide orogeny and later slab roll-back.

A Late Oligocene to Middle Miocene volcanic arc (27-16 Ma) was established between the Peninsular Ranges and coastal Sonoran batholiths, the region that today is occupied by the Gulf of California Umhoefer *et al.,* (2001). Arc magmatism culminated by the end of middle Miocene, marking the end of the subduction process between Farallon and North American plates at the latitude of the Gulf of California. At this latitude subduction was oblique, and relative plate motion in the plate boundary region was partly accommodated by a dextral transtensional system. The time of the tectonic transition from orthogonal basin and range style extension to dextral transtension in the Gulf extensional province (GEP, Figure 1) is, however, controversial.

In general terms, the distinction between the Gulf extensional province from the basin and range proper has not been defined. The GEP is the area between the SMO and coastal Sonora and Baja California (Stock& Hodges, 1989). This region experienced crustal extension in wide-rift mode and core complex formation between 25 and 16 Ma (Wong and Gans, 2008; Nourse *et al*., 1994; Vega-Granillo and Calmus, 2003). Subsequent minor extension continued until 12 Ma and after (McDowell *et al.*, 1997). This extensional episode is coeval with subduction of the Farallon its fragmentation into other microplates, and arc volcanism in Baja California and Sonora. In Baja California, stratigraphic relationships at Sierra San Felipe indicate that transtentional faulting initiated synchronously as a kinematically linked fault system before ~ 7 Ma. This is based on the timing of footwall exhumation, during a phase of rifting that has been called "proto-Gulf"(Seiler *et al.,* 2010).

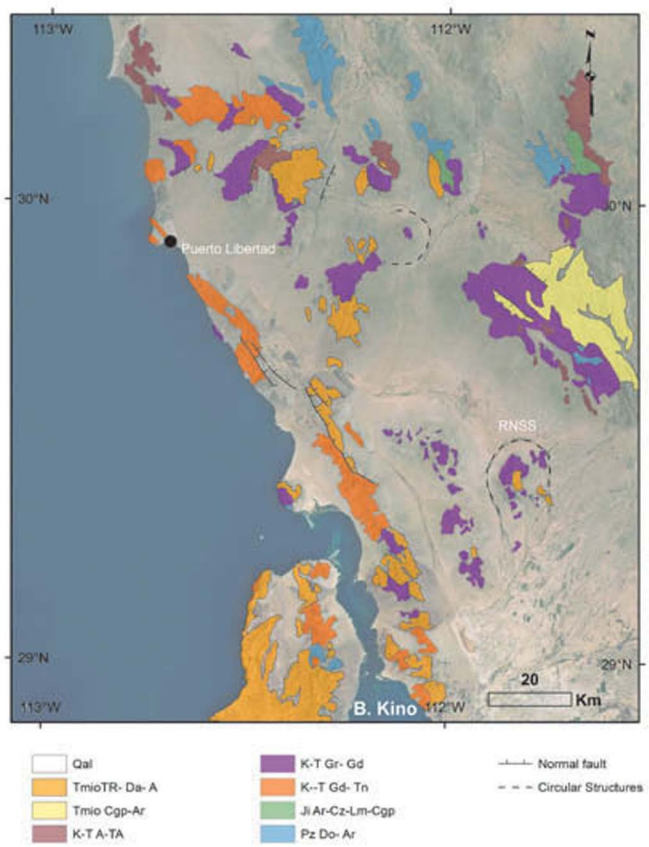

Figure 1. Geologic map of central-coastal Sonora, showing the location of the Rancho Nuevo semi-circular structure. The inset shows the distribution of plutonic rocks assigned to the Peninsular Ranges and the Sonoran Laramide batholithsas well as the Gulf of California extensional province. Modified from Servicio Geológico Mexicano (SGM), 2008. KsGd-Tn=Upper Cretaceous granodiorite and tonalite; KsTpaGr-Gd= Upper Cretaceous-Paleocene granite and granodiorite; JiAr-Cz-Lm-Cgp=Lower Jurassic sedimentary rocks; pTsDo-Ar=Neoproterozoic metasedimentary sedimentary rocks.

The coastal Sonora region hosts the onshore portion of the transform boundary between the Upper Tiburón and Adair-Tepoca marine basins, two early-formed oblique rift segments. Extension commenced here between 11.5 and 7 Ma(Bennett *et al*., 2013). Based on structural, $^{40}Ar/^{39}Ar$ geochronology, and a palinspastic reconstruction Gans (1997) proposed the onset of transtension and relative motion of Baja California together with the Pacific plate shortly after the ~11 Ma termination of subduction.

Correlation of geologic features on both sides of the Gulf of California (Oskin and Stock, 2003a) indicates about 280 km of slip along faults in the gulf, from 6 Ma to present (Atwater and Stock, 1998; Oskin *et al*., 2001). Nonetheless, there are 300 km of dextral motion between the Pacific plate and North America that must be accommodated during the proto-Gulf episode between ~12 and 6 Ma (Stock, 1989; Stock and Hodges, 1989; Stock and Molnar, 1988). Relative plate motion during the proto-Gulf event may have been accommodated west of Baja California by the San Benito and Tosco-Abreojos faults (Stock and Hodges, 1989), east of Baja California along coastal Sonora, or in both (Gans, 1997; Fletcher *et al*., 2007; Bennett *et al*., 2013).

Methodology

This work is based on 1:10,000 field mapping of the RNSS, and detailed petrographic analysis of 50 samples, 16 of which were point-counted for modal analysis (with a minimum of 600 points) for later classification in a Streickeinsen diagram (Streickeinsen, 1976). Structural data were collected at 148 stations, including foliation, lineation, dike orientation, bedding attitude, brittle fault plane, and pitch of striations. Five rock samples were dated using U-Pb geochronological analysis by LA-ICP-MS (Laser Ablation-Inductively Coupled Plasma-Mass Spectrometry). Three samples (T-83, T-91, T-92) were prepared, processed, and analyzed at the University of Arizona, Tucson, using standard techniques that include crushing, sieving, magnetic separation and high-density liquids for final extraction of heavy minerals. Zircon separates were mounted manually in epoxy and polished. Zircons were analyzed in a VGI isoprobe multi-collector ICP-MS, equipped with nine Faraday collectors, an axial Daly detector, and four ion counting channels (Gehrels *et al*., 2006). Two samples (T-205 y TR-46) were processed for zircon separation at the Centro de Geociencias, UNAM Juriquilla Campus, where they were first crushed and sieved, and then subjected to magnetic separation and heavy liquids extraction (MEI). Zircon separates were then manually mounted in epoxy resin and polished. These two samples were analyzed with an ICP-MS Thermo X series "quadrupole" at Centro de Geociencias in Juriquilla Mexico. (Solariet *et al*., 2010).

We collected samples in 27 paleomagnetic sites, all in granodiorite, for a total of 162 samples; the samples have a cylinder shape with 1 inch of diameter and 1 inch high. The same samples were used for anisotropy of magnetic susceptibility measurements (AMS) with the objective of observing if there are changes in the magnetic fabric related to post-emplacement deformation. The sampling was performed with a portable drill using diamond tip drillbits; samples were oriented with magnetic and sun compasses. As with all other field stations, sites were located using a portable GPS device. For magnetic susceptibility measurements we used a KLY-3 Kappabridge susceptibilimeter, using 15 positions. For remanence measurements we used a JR-5 Spinner magnetometer. All samples were subjected to progressive demagnetization, either alternating field demagnetization using an ASC LDA-3 up to inductions of 100 mT or thermal demagnetization using an ASC-TD48 furnace up to temperatures of 590 ºC. The main objective of the paleomagnetic part of this study was to determine a possible rotation or tilt within the RNSS by comparing observed directions with the expected direction from the North America craton reference pole for the Late Cretaceous. All magnetic measurements were performed at the Paleomagnetic Laboratory of the Centro de Geociencias, UNAM Juriquilla Campus. Orthogonal demagnetization diagrams were used to interpret the vectorial composition of the natural remanent magnetization (NRM), and characteristic directions were computed using principal component analysis (Kirschvink, 1980). Site mean directions were calculated using Fisher statistics.

Regional geology

The stratigraphy of western Sonora includes a basement unit composed of various Paleozoic metasedimentary units, with protoliths that range in age from the Cambrian to the Devonian (Gastil and Krummenacher, 1977; Stewart, 1988; Ávila-Ángulo, 1987; Poole, 1993). This assemblage was thrusted over an Upper Paleozoic basin, late in the Ouachita orogeny (Poole *et al*., 2005). Late Cretaceous plutonic rocks of the Sonoran Laramide batholith intruded the entire basement assemblage (Anderson and Silver, 1969; Gastil and Krummenacher, 1977; Valencia Moreno *et al*., 2003; Ramos-Velázquez *et al*., 2008).

The supracrustal units in the GEP in Sonora include four groups after (Oskin and Stock; 2003b, Bennet, 2009; 2013). The oldest, Group I, consists of continental sedimentary rocks of Oligocene-Miocene age. It includes coarse to fine sandstone and conglomerate with basement clasts and clasts of intermediate volcanic rocks. These rocks were deposited by immature fluvial systems and rest unconformably on basement. Group I represents an erosional episode perhaps linked to Basin and Range tectonics within the Gulf of California extensional province.

Group II rocks are likely related to arc volcanic activity associated with the Early- to Middle- Miocene Comondú arc, and subduction of progressively younger Farallon oceanic lithosphere (Umhoefer *et al*., 2001; Gastil *et al*., 1979; Hausback, 1984; Oskin and Stock, 2003b; Bennett, 2009).It consists of volcanic flows and pyroclastic deposits of intermediate composition. Although the tuff of San Felipe is included in Group II, and represents the onset of extension in the northern GEP, and it clearly postdates the end of subduction and arc volcanism (Stock *et al*., 1999; Vidal Solano *et al*., 2007; 2008). The tuff of San Felipe (Ttsf) is a regional stratigraphic marker that covered an approximate surface of >4000 km^2 on both margins of the Gulf of California. Distribution of the Ttsf has been used as a piercing point for reconstruction of the peninsula to its pre-opening position because the age of Ttsf is 12.5 Ma (Oskin, 2002; Oskin and Stock 2003a). The Ttsf crops out in the RNSS with a thickness of 60 m (Figure 2).

Group III consists of basaltic and rhyolitic rocks interstratified with non-marine strata. It is Middle Miocene to Late Miocene (11.47-6.39 Ma), (Oskin *et al*., 2003b; Bennett etal., 2007). The upper age of Group III is considered late Miocene, based on the age of the Mesa Cuadrada tuff of 6.39 ± 0.02 Ma, $^{40}Ar^{39}Ar$, in plagioclase, published by Bennett *et al*. (2007). Group III includes ignimbrites regionally distributed over an area >2100 km^2 on both margins of the Gulf, in Isla Tiburón, (Oskin and Stock, 2003a, b), and in coastal Sonora (Oskin *et al.*, 2001). Mesa Cuadrada tuff deposits are thin, about 30 m. Characteristics of this unit that makes it easily recognizable are that it changes laterally from non-welded to poorly welded, and it presents a conspicuous salmon color. The series of rocks deposited between the San Felipe and Mesa Cuadrada tuffs, between 12.5-6.4 Ma (Stock *et al*., 1999),may contain the geologic record of transtension in the Gulf of California. Finally, Group IV consists of sedimentary rocks, characterized by non-marine strata with local intercalations of pyroclastic deposits such as air-fall tuffs. These strata were deposited during the latest proto-Gulf stages (Pliocene-Holocene). Coastal eolian and beach deposits, as well as alluvial and fluvial strata also included in Group IV.

Geology of Rancho Nuevo Semicircular Structure

The RNSS is located in the Sonoran coastal plain, about 160 km NW of the city of Hermosillo and about 40 km from the coast. RNSS is composed of granitic rocks that intrude an andesite unit mapped as part of the Sonoran Laramide batholith. The RNSS is a domo shaped geomorphic feature defined by conspicuous drainage patterns. The dome may have been produced by a magmatic chamber, or with later erosion. The structure is an elongated dome, with a 30 km long axis, oriented nearly N-S, and it is about 15 km wide. The arroyos (ephemeral streams) draining small and apparently disorganized sierras outside the structure run into a loop that surrounds the structure, whilst drainage runs radially away from the core of the structure into the same loop. Drainages eventually collect south of the RNSS and flow into playa San Bartolo. The RNSS is cored by suite of Late Cretaceous intrusive rocks (Figure 2). For the description of the geology of the RNSS, we grouped rocks chronologically associated with the Late Cretaceous intrusive suite, and rocks associated with the Miocene volcanic and volcaniclastic sequence.

Late Cretaceous intrusive and volcanic rocks at Rancho Nuevo

The Cretaceous suite at the RNSS is composed of plutonic rocks and their host rock. The host rocks are Late Cretaceous, greenish gray andesite flows. These lava flows crop out primarily in the south-central sector of the structure, forming low-standing hills (Figure 2). The andesite unit is intruded by plutonic rocks which include four units: (1) granodiorite-monzogranite, (2) monzogranite, (3) quartz-feldspathic porphyry, and (4) quartz-rich granitoid, aplitic and pegmatite dikes. Near the contact with the intrusions the andesite unit it develops neoformations zones, or andesite breccias at greater distance from the contact. The mineralogy of andesite flows consists of plagioclase > pyroxene + chlorite and Fe-oxides.

The granodiorite-monzogranite unit is the largest of the intrusive suite because of its volume and areal extend. It is also important because this unit has a sigmoidal fracture pattern, which

is described in the next section. This pattern is further emphasized by the intrusion of a series of Miocene rhyolitic dikes (Figure 2). Outcrops of the granodiorite-monzogranite unit form valleys between minor and discontinuous north-south ranges where plutons of more felsic composition crop out. The granodiorite-mozogranite unit is light to dark gray depending on mafic mineral content. Microscopically, the quartz presents undulatory extinction, and

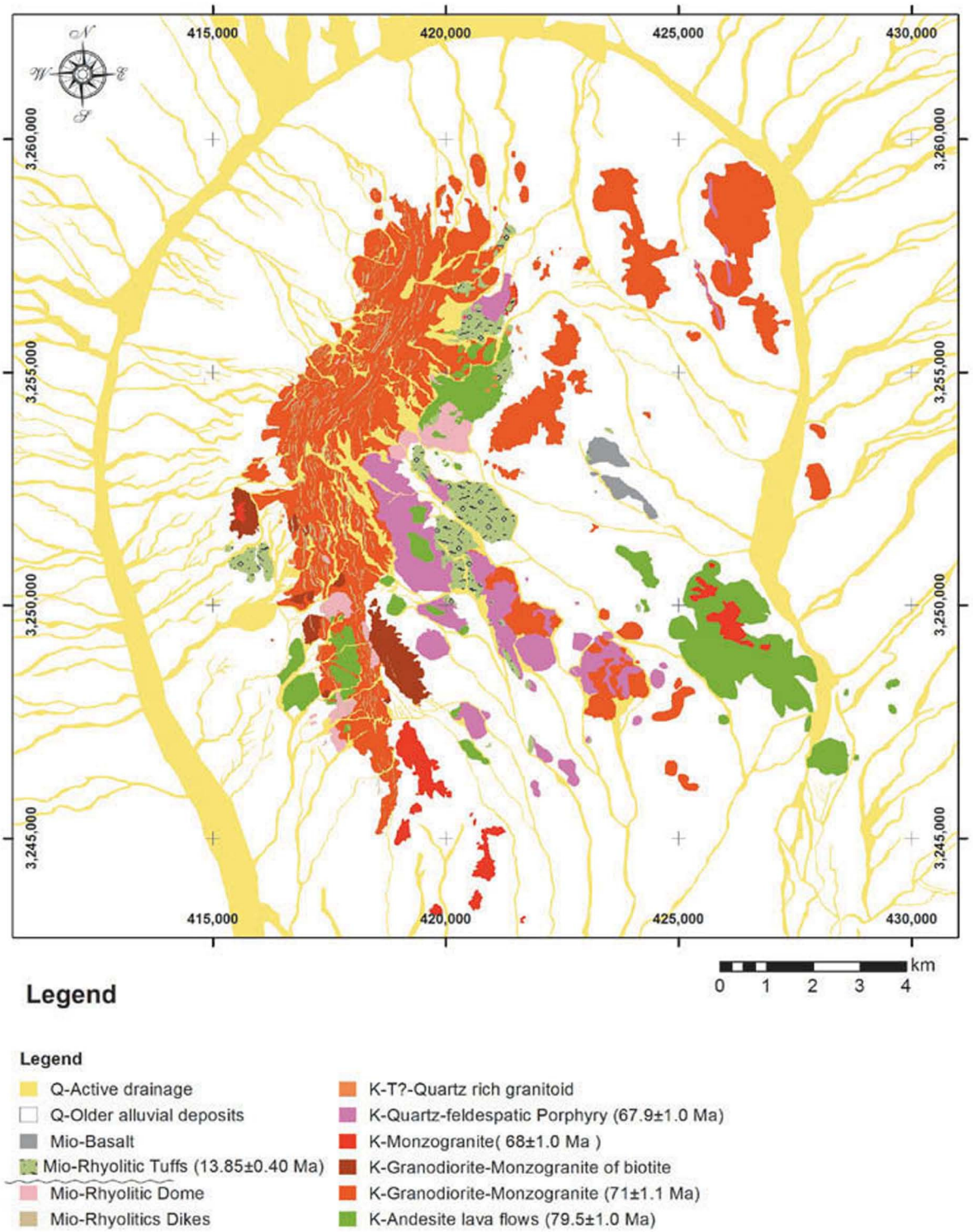

Figure 2. Generalized geologic map of Sierra Rancho Nuevo.

the plagioclases are often fractured or broken forming a matrix of small crystals with quartz and feldspar recrystallization. The biotite abundance increases in zones of hydrothermal alteration. Amphiboles are often corroded, and also altered to chlorite and epidote. Potassium feldspar content gradually increases to the east of the RNSS, where the composition changes transitionally from granodiorite to monzogranite. (Figure 3 and Appendix I).

The granodiorite-monzogranite unit is intruded by coarse-grained monzogranite unit. Characterized by a distinctive texture of large feldspars phenocrytals and marked mineral lineation and in outcrop it presents a pinkish coloration due to K-feldspar content and biotite oxidation. The monzogranite crops out on the southern and western sides of the structure (Figure 2). The monzogranite presents various families of fractures with different orientations, which are often filled by aplitic dikes and pegmatites. Locally, the monzogranite includes granodiorite xenoliths, which lack reaction rims and do not present preferential orientation. Xenoliths may be as much as 20 cm in diameter but are generally between 5 and 10 cm. In thin section, this rock is composed of quartz with undulatory extinction, both microclines and orthoclases are 1 to 2 cm in length, plagioclase crystals are not zoned but a number of them are broken up or deformed as kink-bands. Plagioclase rims are often corroded and show quartz-feldspar recrystallization. This is often a feature produced by crystal-plastic deformation (Vernon, 1975). Many biotite and amphibole crystals are altered to chlorite, epidote and Fe-oxides.

The quartz-feldespatic porphyry unit crops out in the south-central part of the RNSS, forming small hills. To the northeast of the structure, the porphyry intrudes the granodiorite-monzogranite unit in the form of dikes with a preferred orientation 10° to 20° NW (Figure 2). Quartz and K-feldspar crystals are embedded in an aphanitic matrix. Potassium-feldspar (orthoclase) is commonly broken up and shows sericitic alteration. Many plagioclase crystals are zoned. Biotite grains are euhedral; most of them are fractured, corroded, oxidized and sericitized. There are small amounts of hornblende altered to epidote, chlorite and Fe-oxides.

The granite rich in quartz, aplite and pegmatite dikes unit is the kind of facies typically associated with late crystallization phases in the magma chamber. The granite bodies are scarce within the RNSS, cropping

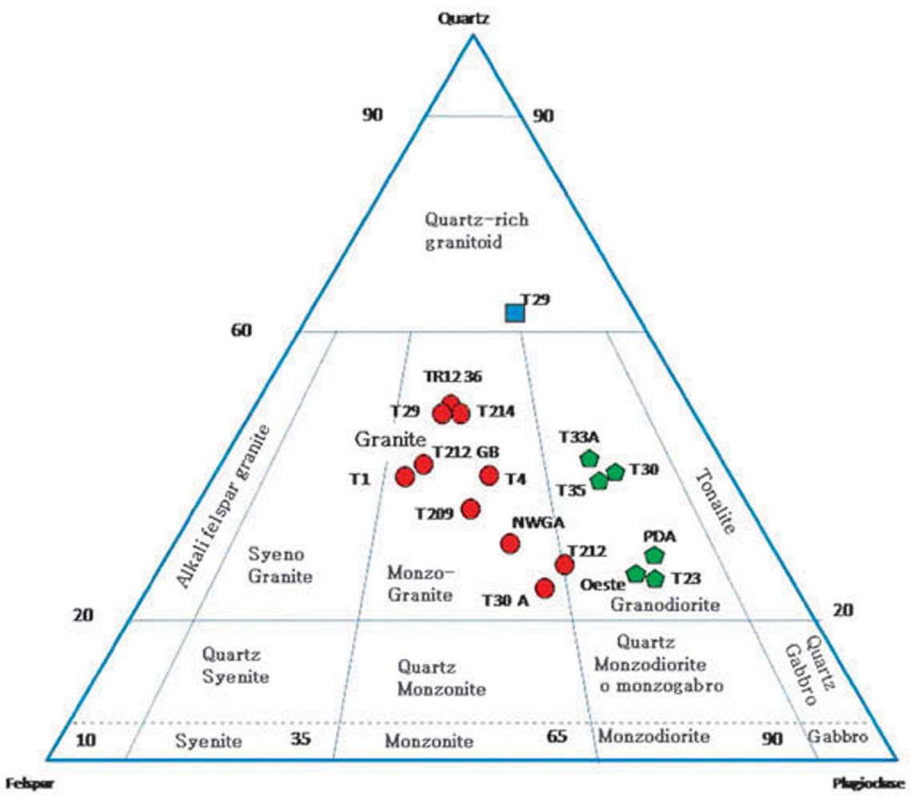

Figure 3. Intrusive rocks classification diagram, Streickeisen (1976), shows the representative samples distribution of RNSS units. The original data are summarized in Appendix I.

out as scattered apophyses not larger than ~100 m in diameter. They are light gray and of fine-grained texture. The aplitic and pegmatites dikes are generally less than 1 m thick, and show no preferred orientation. More common mineralogical association in these dikes is quartz, potassium-feldspar, plagioclase, mica, and accessory tourmaline.

The Miocene volcanic and sedimentary rocks

Miocene volcanic and intrusive rocks in the RNSS either unconformably overlie the Cretaceous plutons or intrude in to them. They were mapped as three compositional units: rhyolite lava, rhyolitic tuffs, and basalts flows. The rhyolite unit includes dikes filling sigmoidal fractures within the granodiorite-monzogranite main pluton, as well as associated domes which are coeval. The rhyolite dikes occur mostly in the western side of the RNSS, but dikes cut the entire structure from north to south; they also occur in the central-eastern side and cut quartz feldspatic porphyry (Figure 2). The dikes form as discontinuous prominent ridges, rising tens of meters above their surroundings. As mentioned earlier, rhyolites dikes follow sigmoidal trends striking N-S in the north, NE-SW in the center, and NNW in the south. The sigmoidal fracture pattern that they intrude was developed earlier or during the emplacement of the rhyolitic dikes within the granodiorite-monzogranite. The rhyolite dikes are ~ 2 km long, but they are narrow (2-4 m). The rhyolite unit also includes domes up to 400 m in diameter. Generally they are pink to reddish-gray because of the presence of Fe-oxides. They have an aphanitic texture, containing <5% of quartz, feldspar or plagioclase phenocrysts.The rhyolite also contain small crystals of fayalite, aegirine (<1%), and arfvedsonite (<1%), which are indicators of high alkaline composition (Vidal-Solano, personal communication 2012).

Dispersed across the RNSS, there are outcrops of volcanic and volcaniclastic rocks mapped as the rhyolitic tuff unit. These rocks generally occur as small remnants, filling paleo-valleys between minor ranges composed of granitoid. The largest outcrops are about 3 km^2 in the east-central side of the RNSS. The base of the volcaniclastic sequence is formed by tuffaceous breccias, which include clasts of the volcanic and granitic older units, overlain by a well-stratified volcanic sequence. This sequence is composed of ~18m thick a black vitrophyre, lapilli tuffsof rhyolithic composition, ~20 m of pinkish lithic tuff of rhyolitic composition, about 3m of clear fine-grained tuff (pumicite), and a second vitrophyre 4m thick. The sequence overlies ~18m of pinkish and yellowish tuff for a total thickness of about 60 m. This unit is gently tilted, 5°-18° to the west, probably produced by the paleo-geography. The petrological characteristics of this unit suggest that it may correlate with the tuff of San Felipe. The basalt unit in the map (Figure 2) is restricted, to isolated outcrops scattered along the RNSS; however, the contact with the underlying intrusions is not well exposed. In the central part of the structure basalts flows dip gently ~10° to the northeast.

Geochronology

Five samples within the RNSS were selected for U-Pb zircon dating. Analytical results are summarized in Appendix 2, and results are summarized in Figure 4 and Table 1. An isotopic age of 79.5±1.0 Ma (Campanian) was obtained for sample T205 of the andesite unit, host rock to the Rancho Nuevo intrusive suite. The age is based on the average of 11 concordant grains. The zircon analysis of the intrusive rocks yielded ages of 71±1.1 Ma (sample T92, from granodiorite-monzogranite, average of 27 concordant grains), 68±1.0 Ma (sample T91, monzogranite, average of 24 concordant grains), and 67.9±1.0 Ma (sample T83, quartz-feldspar porphyry, average of 24 concordant grains). The ages obtained are consistent with field relations, as the granodiorite-monzogranite is intruded by the younger granitic and subvolcanic units. A rhyolitic feeder dike yielded a crystallization age of 13.2±0.4 Ma (Figure 4, and Table 1) based on the average of 10 concordant grains.

Structural observations

The Rancho Nuevo granodiorite-monzogranite unit contains sigmoidal fractures hundreds to tens of meters long, where most of the fractures were filled by viscous rhyolite. These fractures were clearly formed after pluton emplacement. The sigmoidal pattern of fractures and rhyolite dikes is clearly visible on satellite images of high resolution. Figure 5. The fractures and dikes are nearly vertical (79°-90°). In the north, fractures and dikes strikes are predominantly 20°-30° to NE (Figure 6a), and change orientation to 0°-10° NNE in the central portion of the range (Figure 6b), whilst in the south fractures and dikes strike 0°-10°NNW (Figure 6c). Figure 6d shows the strike of the complete data set, with a resultant strike. The geometry of the fractures and dikes in the RNSS resembles an *en-echelon,* dextral-shear indicator, formed in a brittle-ductile environment. Apparently, the continuation of the Rancho Nuevo sigmoidal struture is buried by alluvial deposits south and north of the RNSS (Figure 2).

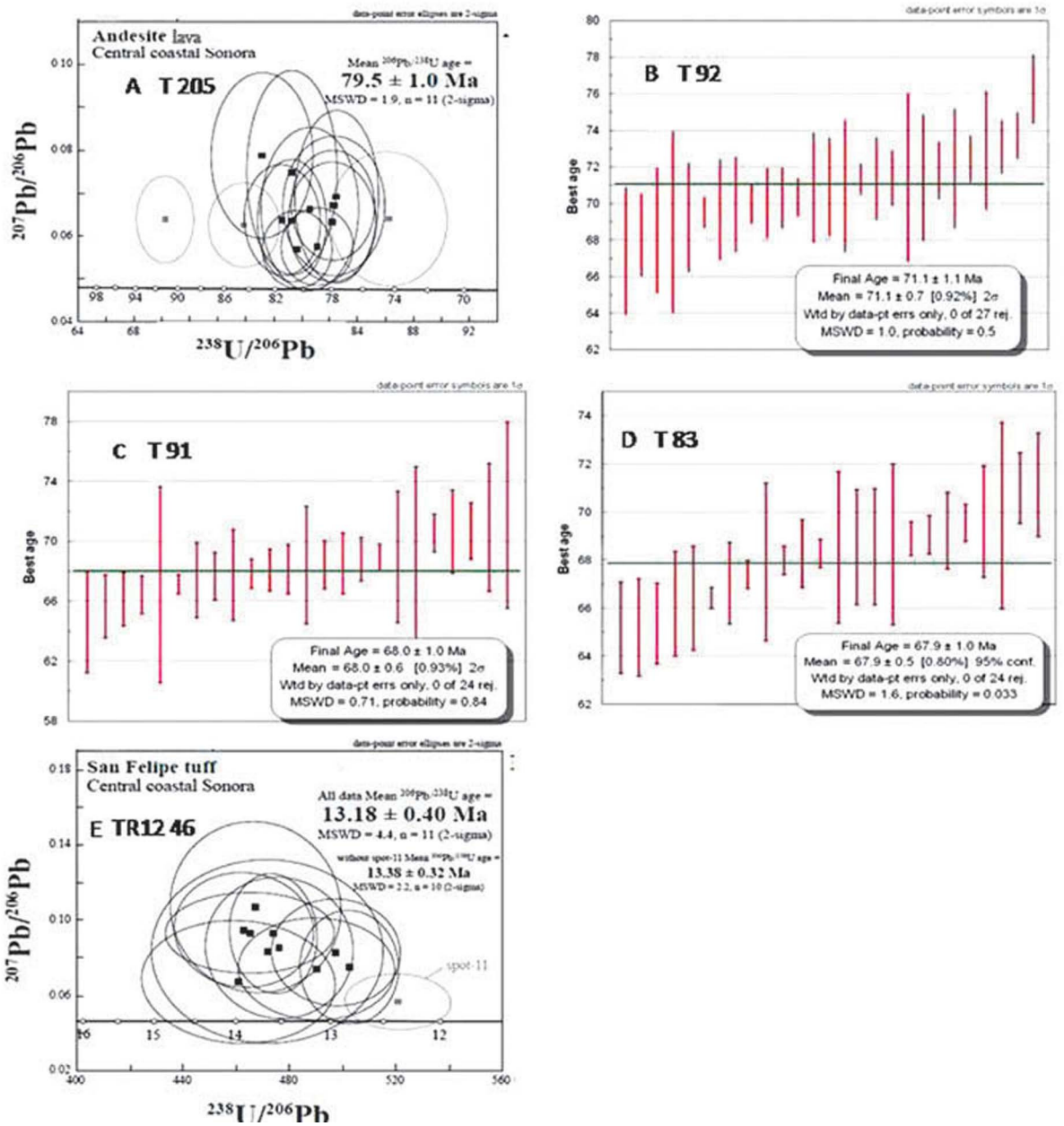

Figure 4. Geochronology results of samples from Sierra Rancho Nuevo by U-Pb LASER ablation method in zircon. the samples (T-92, T83, and T91) were analyzed at Arizona University. The samples (T-205, TR12 46) were processed at Universidad Nacional Autónoma de México, Campus Juriquilla.

Table 1. Summary of geochronological data.

Sample	E Coordinate	N Coordinate	Unit	Age (Ma)
T-205	419812	3243269	Kand	79.5+/-1.0
T-92	425877	3257407	Gd-mzgr	71.1+/-1.0
T-91	425404	3257313	Kpor	67.9+/-1.0
T-83	420614	3243460	KMz	68.0+/-1.0
TR12-46	423440	3253799	Dike	13.2+/-0.4

The granodiorite-monzogranite body does not display a macroscopic foliation or mineral lineation, nor ductile shear zones. Other kinematic indicators are striations in the internal faces of the factures where rhyolite dikes were emplaced. These observations combined with observations of microscopic brittle deformation and plagioclase recrystallization, suggest that deformation occurred at relatively shallow crustal levels. The coarse-grained granite unit in the southern extreme of the RNSS is characterized by variable but nearly N-S magmatic foliation defined by feldspatic phenocrystals that deep steeply >70º to the east.

Anisotropy of magnetic susceptibility

Because of the scarcity of kinematic indicators and the homogeneity of the Cretaceous granitoids, we employed anisotropy of magnetic susceptibility (AMS) as an estimate of strain recorded by intrusive rocks of the RNSS. AMS fabric often parallels the orientation of the strain ellipsoid, but interpretation may not be straightforward. AMS fabrics are represented by an ellipsoid defined by the axis of maximum, intermediate and minimum susceptibility (kmax, kint, and kmin). The maximum and intermediate axes define the magnetic foliation plane, while the shape of the ellipsoid is described using relations between the axes in terms of the parameter T (T<0 for prolate ellipses, and T>0 for oblate ellipses). The intensity of the fabric is evaluated with the percentage of anisotropy (Pj) parameter (Table 2).

AMS studies have been applied to the systematic study of plutonic rocks, which generally have relatively simple magnetic mineralogy (Borradaile, 1988; Borradaile and Henry, 1997). The interpretation of these data, however, can be difficult because the magnetic susceptibility ellipsoid often reflects the combination of emplacement related strain (due to magma flow or interaction with the host rock), regional strain during emplacement, as well as solid-state deformation after emplacement.

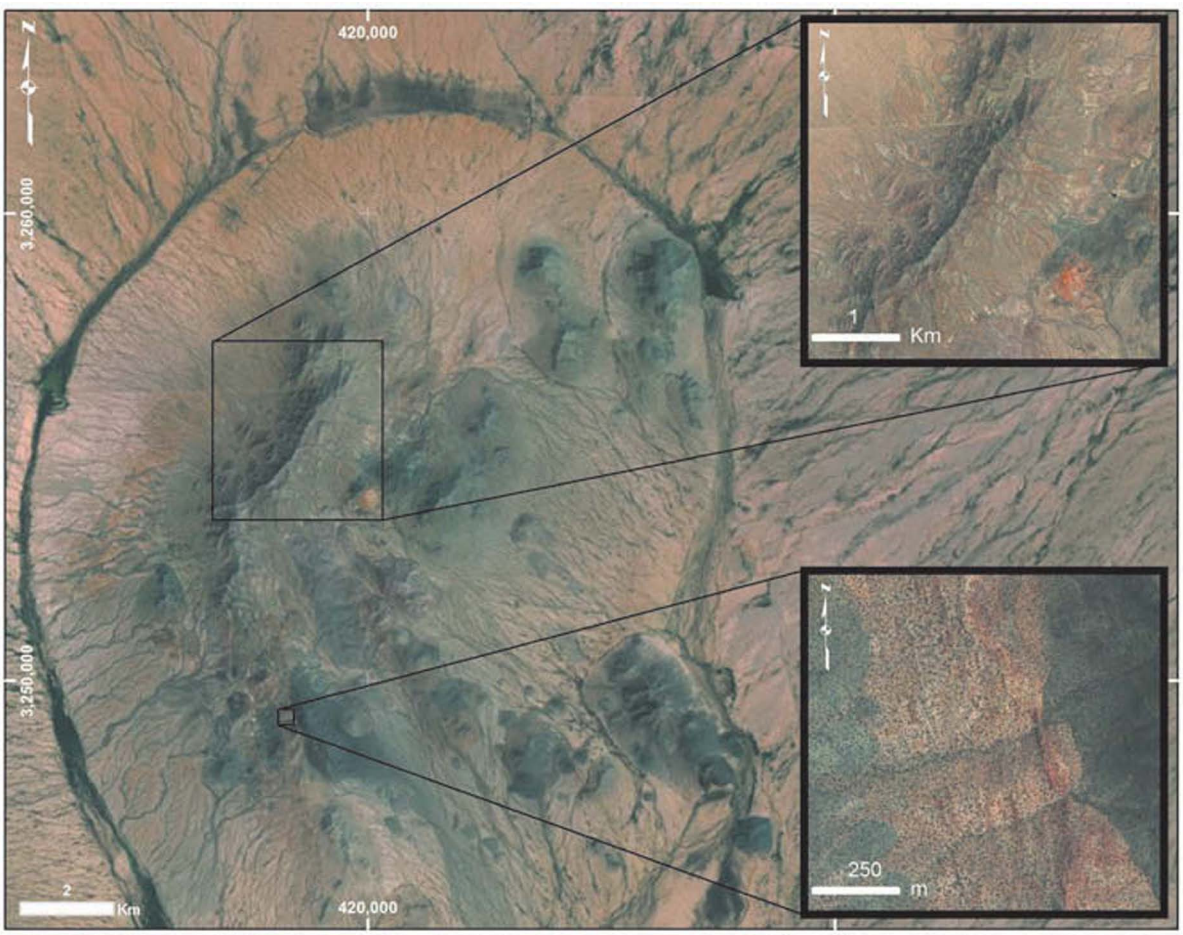

Figure 5. Shows the RNSS and the system of fractures filled of rhylitic composition dikes. Two detailed images of the dikes in the northern and southern portion are presented. Images taken of Google Earth.

Table 2. Summary AMS data of RNSS.

Site	N	Kmean	K1	K2	K3	Dec K1	Dec k2	Dec k3	Inc k1	Inck2	Inck3	L	F	P	Pj	T	U
RN1	12	1.18 e-2	1.004	1.001	0.995	339.7	79.1	242.3	8.4	47.7	41.1	1.003	1.007	1.01	1.01	0.385	0.383
RN2	9	2.91 e-2	1.066	1.056	0.878	46.9	315.2	139.8	2.2	37.4	52.5	1.009	1.204	1.215	1.246	0.907	0.898
RN3	6	2-66 e-2	1.023	1.015	0.962	50.9	161.3	315.6	10.7	61.4	26.1	1.008	1.0055	1.063	1.069	0.741	0.734
RN4	9	1.09 e-2	1.014	1.004	0.982	222.4	45.7	313.5	35.6	54.3	1.6	1.01	1.022	1.032	1.033	0.389	0.383
RN5	12	6.58 e-3	1.016	0.998	0.986	53.7	173.9	320.1	11	68.9	17.8	1.018	1.012	1.03	1.03	-0.213	-0.220
RN6	13	2.03 e-2	1.017	1.008	0.975	6.4	248.4	99.6	9.9	69.5	17.8	1.01	1.033	1.043	1.045	0.547	0.54
RN7	9	1.81 e-4	1.006	1.002	0.992	100.1	241.7	8.2	11.7	75.2	8.9	1.003	1.01	1.013	1.014	0.488	0.485
RN8	10	1.82 e-2	1.028	1	0.972	167.3	76.3	333.9	15.3	3.4	74.3	1.028	1.028	1.058	1.058	-0.002	-0.016
RN9	7	2.94 e-2	1.019	1.003	0.978	262.8	170.8	75.6	31.9	3.2	57.9	1.016	1.025	1.042	1.042	0.222	0.212
RN10	9	3.06 e-2	1.04	0.993	0.967	207.9	69.2	327.9	54.4	28.6	19.9	1.047	1.027	1.075	1.076	-0.226	-0.283
RN11	7	5.57 e-2	1.027	0.989	0.984	190.8	100.5	283	0.08	20.2	69.8	1.038	1.006	1.044	1.047	-0.74	-0.745
RN12	7	1.53 e-2	1.017	0.997	0.986	40	298.4	180.4	29.8	19.3	53.4	1.019	1.011	1.031	1.031	-0.252	-0.259
RN13	7	1.75 e-2	1.011	1.004	0.984	169	289.4	76.7	8.7	73.2	14.3	1.007	1.021	1.028	1.029	0.497	0.492
RN14	6	1.19 e-2	1.017	1.003	0.98	9	244.9	129.8	39.5	34.3	31.9	1.014	1.023	1.038	1.038	0.224	0.215
RN15	10	1.68 e-2	1.032	1.001	0.966	74.5	225.1	323.4	56	30.5	13.7	1.031	1.037	1.069	1.069	0.081	0.064
RN16	7	1.72 e-2	1.026	0.998	0.976	41.3	282	133.1	7.2	74.6	13.6	1.028	1.022	1.051	1.051	-0.11	-0.122
RN17	9	1.67 e-2	1.026	0.999	0.975	196.6	303.6	94.5	14.9	47.8	38.4	1.027	1.024	1.053	1.053	-0.057	-0.07
RN18	8	2.1 e-2	1.028	0.999	0.973	111.3	4.7	263.4	48.6	14.1	37.9	1.028	1.027	1.056	1.056	-0.031	-0.044
RN19	8	9.12 e-4	1.01	0.998	0.992	168.8	69.5	265	7.7	50.3	38.6	1.012	1.006	1.018	1.018	-0.342	-0.346
RN20	8	1.99 e-2	1.032	1.017	0.95	113.9	258.2	354	63.4	22.1	14	1.014	1.071	1.086	1.092	0.653	0.641
RN21	6	1.24 e-2	1.013	0.994	0.993	92.2	329.2	213.1	38.6	34.3	32.8	1.019	1.001	1.02	1.023	-0.864	-0.865
RN22	6	2.2 e-2	1.015	0.998	0.987	195.7	311.5	80.3	28.6	38.6	38.2	1.017	1.011	1.029	1.029	-0.229	-0.236
RN23	7	4.74 e-3	1.011	1.005	0.983	150.5	35.2	301.5	67.5	10	20	1.006	1.023	1.029	1.03	0.578	0.573
RN24	7	6.97 e-3	1.011	1.003	0.987	199.1	353.1	94	48	39	13.1	1.008	1.016	1.024	1.025	0.337	0.331
RN25	7	5.45 e-3	1.011	1.007	0.982	178.9	357.8	88	69.7	20.3	0.3	1.003	1.026	1.03	1.032	0.772	0.769
RN26	6	1.24 e-2	1.02	0.999	0.981	354	120.6	211.2	82.2	4.7	6.2	1.021	1.018	1.039	1.039	-0.06	-0.069
RN27	6		1.006	1.002	0.991	291.5	142.4	36.2	41.4	44.3	16.1	1.004	1.011	1.015	1.016	0.452	0.449

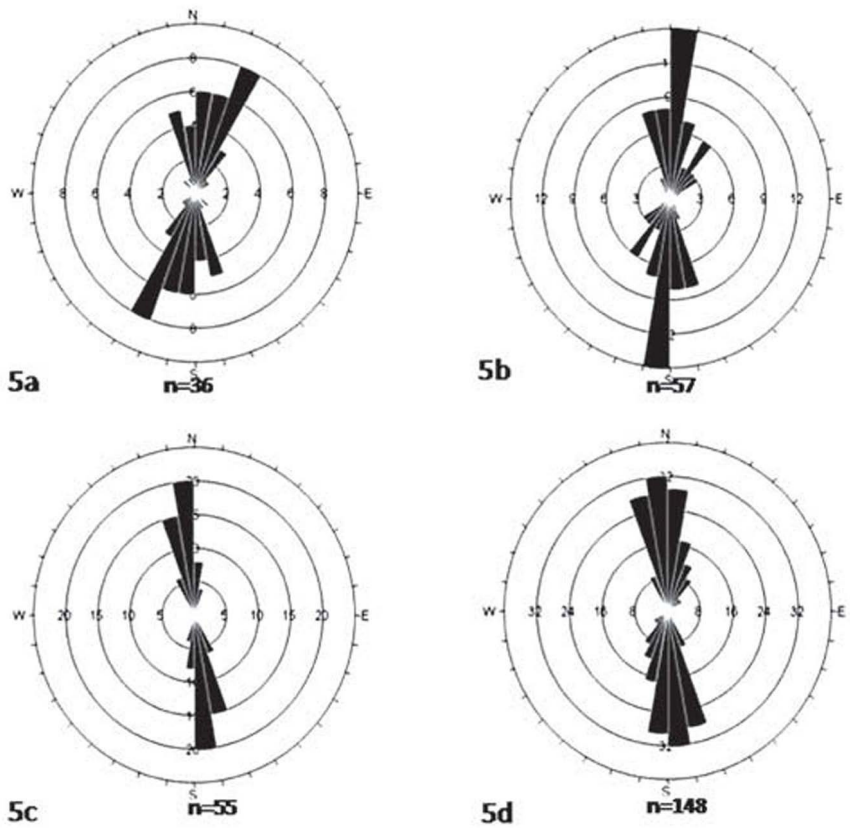

Figure 6. Diagrams of representations main strikes (rhyolitic compositions dikes) about different sectors in RNSS.5a) North sector, 5b) Central sector, 5c) South sector, and 5d) all data sectors.n=collected number data.

AMS data were obtained in all 27 drilled sites. The samples were measured prior to beging demagnetized, Magnetic susceptibility for samples of the granodiorite-monzogranite are high, with the mean of the samples ranging between about 5 $x10^{-3}$ and 6 $x10^{-2}$ SI units, except for sites 7 and 19 that have significantly lower values (between 1 and 9 $x10^{-4}$). The high susceptibility values suggest that the magnetic fabric is dominated by the ferromagnetic mineral phases (Ellwood and Wenner, 1981). Despite the fact that the granodiorite-monzogranite unit does not display a visible fabric, there is a weak but well-defined magnetic fabric. Percentage anisotropy is relatively low, with an average value of 1.048 (typical of undeformed to weakly deformed granitoids), but with a wide range between 1.010 and 1.246; the high values suggest that high strain is recorded at some sites. The highest values of percent anisotropy (Pj>1.06) were observed in the northern and eastern sides of the mountain range. The shape parameter T varies within the Rancho Nuevo sigmoidal structure. Four sites in the central part of the RNSS have a range of T between -0.002 and -0.11, indicating nearly tridimensional to weakly prolate ellipsoids (Figure 7, Table 2). In the northern and southern sectors of the structure, ellipsoids are dominantly prolate (at six sites T ranges between -0.252 and -0.864). Nonetheless, at rest of the sites T typically has positive values indicating ellipsoids of oblate shape. Oblate ellipsoids suggest generally SE-NW to NE-SW compression.

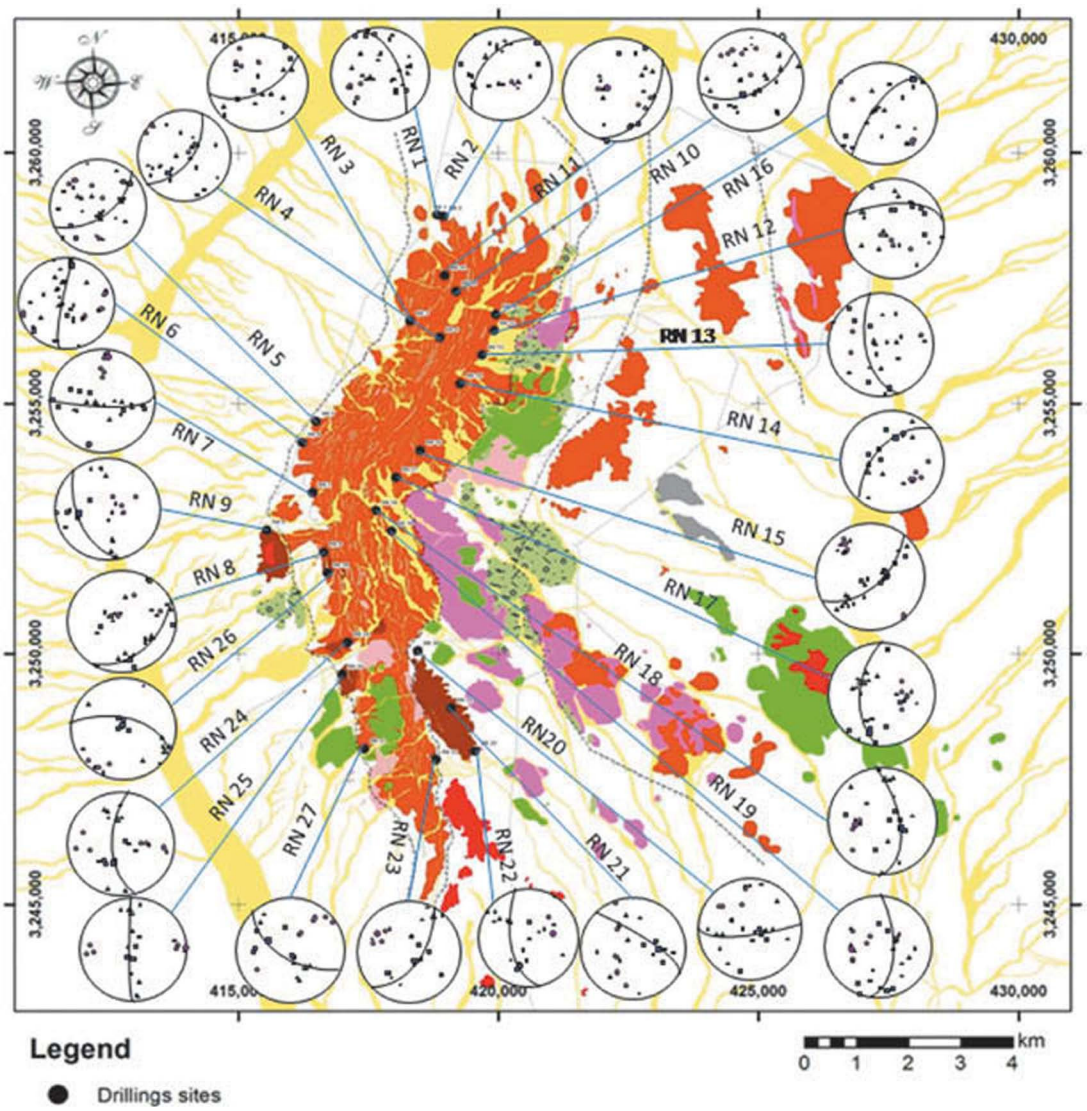

Figure 7. Drilling sites for paleomagnetism and magnetic fabric, the stereograms represent the graphics (AMS) in lower hemisphere. Squares correspond to maximum, triangles to intermediate, and circle to minimum susceptibility axes. The black line symbolize average magnetic folitation plane for each particular site in granodiorite-monzogranite unit.

The orientation of kmax, kint and kmin is displayed in Figure 7. The orientation of the AMS foliation in the granodiorite-monzogranite unit is generally parallel to the dike orientations, such as in sites 13 through 17 in the NE side of the sigmoid, sites 6 and 11 in the northern side, and sites 21 to 25 in the southern sector of the sigmoid (Figure 7). There are, however, significant deviations with foliation planes oblique to the structure, such as sites 20 and 21, as well as 7. These sites generally show the lowest percentage anisotropy values (<1.015), suggesting they were not affected significantly by deformation after emplacement. Magnetic lineation, interpreted from kmax, suggests roughly a NNE-SSW direction and small elongation in the northern part of the RNSS, and N-S and moderately steep in the southern part.

Paleomagnetism

Samples of the granodiorite-monzogranite collected at Rancho Nuevo generally have moderately strong magnetizations, and relatively straightforward demagnetization behavior. The NRM is typically the sum of two magnetizations. A low coercivity magnetization is removed with inductions of about 12 mT (Figure 8). The directions of the low coercivity component show no prevalent within-site orientation. A moderate-coercivity (20-80 mT) magnetization is defined by linear trajectories to the origin, and it is considered the characteristic magnetization (ChRM). The direction of the ChRM is typically to the SW and moderately steep negative, or antipodal to this direction, but it is to the southwest and shallow at three sites in the north and the west sides of the structure and to the NW (SE) and moderately steep positive (negative) at sites 9 and 19 (Figure 8, Table 3). A ChRM was identified at 16 sites, but in one of them the statistic is poor. Within-site dispersion of the ChRM is low, with precision parameter generally higher than 50. At eleven sites no stable magnetization was observed. In some of these sites the NRM is of very low coercivity, and directions within a site have high dispersion; in others demagnetization behavior is erratic. The ChRMin 15 sites are predominantly of reverse

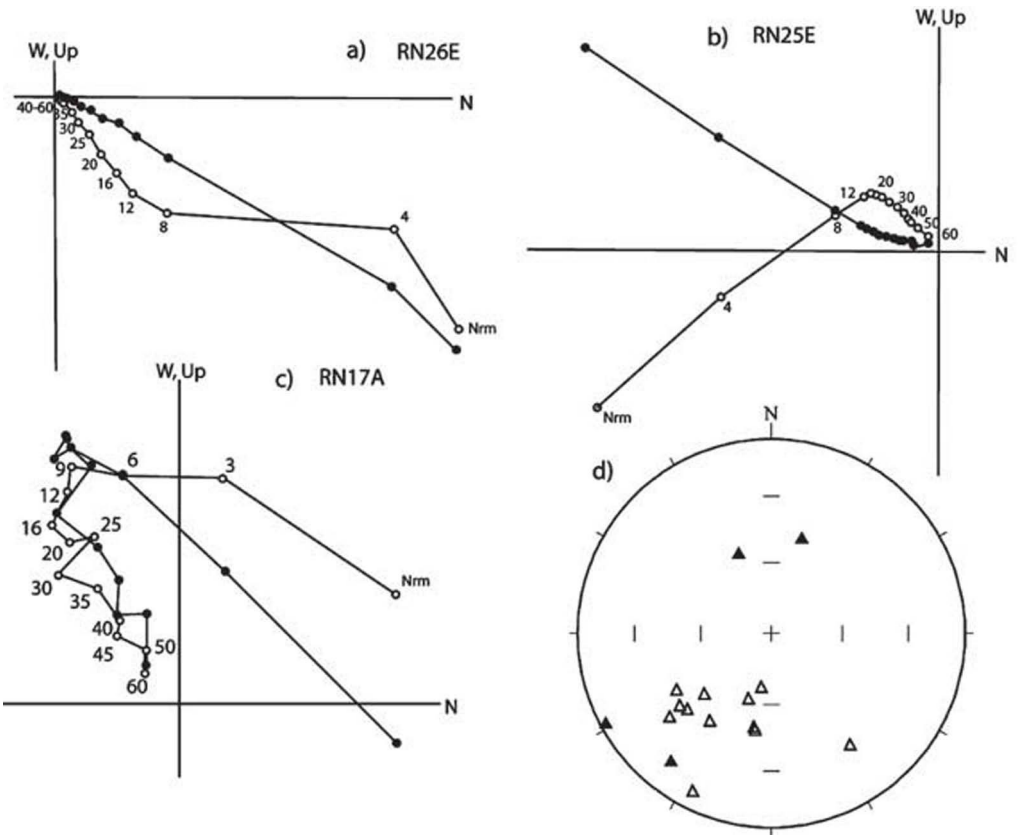

Figure 8. Paleomagnetic data. (a-c) Orthogonal demagnetization diagrams of selected samples. Open (closed) symbols are projections on the vertical (horizontal) plane. (d) Stereographic projection of the characteristic magnetization (in situ), here open (closed) symbols are projections on the upper (lower) hemisphere.

Table 3. Paleomagnetic data and statistical parameters.

Site	n	Dec (º)	Inc (º)	k	a95	Dec (º)	Inc (º)
rn1	1	204.9	-13.7			202.6	-12.6
rn5	3	233	2.4	76.9	14.2	233.1	-1.5
rn6	4	211.6	16.7	162.6	7.2	214.6	16.2
rn9	3	146.8	-37.4	44	18.8	144	-28
rn15	3	247.3	-41.1	76.3	23.4	240.1	-46.4
rn16	5	236.4	-35.1	20.0	17.5	229.4	-39
rn17	6	233.9	-49.5	288.7	3.9	222.1	-52.6
rn18	6	231.5	-48.4	46.0	10.0	220.1	-51.1
rn19	2	341	55.1			333.5	47.1
rn20*	6	185.4	-68.3	10.9	21.3	167.1	-62.7
rn21	6	233.7	-59.6	393.2	3.4	216.2	-62.2
rn22	4	199.5	-62.4	54.7	12.4	182.5	-59.1
rn24	6	197.5	-49.3	152.9	5.4	187	-46.2
rn25	6	196.8	-47.1	505.6	3.0	187.1	-44
rn26	6	21.3	44.6	498.7	3.0	12.1	42.3
rn27	3	211.4	-43.3	203.8	8.7	202.1	-42.7
Mean	**10**	**219.7**	**-49.5**	**28.4**	**9.2**	**207.9**	**-50.2**

Here n is the number of samples used in the calculation of the site mean.
Dec and Inc are the declination and inclination, with statistical parameters k and alpha 95. Dec+ and Inc+ correspond to tilt corrected directions.

polarity, consistent with emplacement during C31r. based on the average age of ~70 Ma, for granitoids.

Between-site dispersion appears high, but a group of ten sites yields a well defined mean direction of D=219.7º and I=-49.5º (k=28.4 andα_{95}=9.2º); this calculation includes most of the sites in the southern and eastern sides of the structure. Corrected for the gentle westward tilt of the Miocene tuffs near El Volteadero ranch in the center of the structure, the direction is D = 207.9º and I = -50.2º. The ChRM is discordant with respect to the direction calculated for the sampling locality from the North America reference pole, which is D = 166.1º and I = -56.9º (based on Besse and Courtillot, 2002). The mean direction indicates clockwise rotation of 41.8º+/-11.6º, with small flattening (F=6.7º+/-3.4º). For individual sites, calculations of R(rotation) range between about 16º and 74º. It appears, however, unlikely that the RNSS rotated as a rigid body, as sites in the north and west with southwesterly and shallow ChRM indicate a combination of rotation and tilt (southward), and two sites (9 and 19) do not record significant rotation.

Discussion

To our knowledge, this is the first study where the deformation of intrusive rocks in the extensional province of the gulf is analyzed. The most evident indication of deformation in the RNSS is the presence of a sigmoidal structure, which later on was filled by viscous rhyolite as dikes.The sigmoidal structure appears to have been produced by the gash extensional fractures (σ3) which are perpendicular to the maximum stress (σ1, Figure 9). The fractures may be rotated by ductile deformation either during or after formation. As gash fractures develop at different times of ductile shearing they show different amounts of rotation. This deformation coincides with the results of the paleomagnetic study.

The AMS is a technique that defines the orientation and intensity of the magnetic fabric in the rocks. The AMS in the granodiorita-mozogranite unit of the RNSS shows that considerable changes in the orientation of the magnetic fabric exist in the rock, indicating that they record significant strain. Also, the characteristic magnetization of the granodiorite-monzogranite is discordant with respect to the expected direction; the discordance is best explained by rotation about a local nearly vertical axis of about 40º. As mentioned above, not all sites record the same amount of rotation. For instance, sites 5 and 6 in the western side of the structure require a combination of rotation and tilt. This suggests that the structure did not behave as a rigid body during deformation. Based on the crystallization age (U-Pb) for the dikes of rhyolite, which are considered coeval

or little younger than the dextral transtentional deformation, we conclude strike-slip deformation occurred by about 13 Ma.

Prior to ~16 Ma, the southwestern edge of the North American plate along northwestern Mexico was a subduction boundary (Fig. 2A; Atwater, 1970). By ~12.5 Ma, the Rivera-Pacific-North America triple junction jumped southeastward, setting the stage for transfer of the Baja peninsula to the Pacific plate. Karig and Jensky (1972) proposed that prior to the gulf existed in the area in the earliest stages of rifting from ca. 14 to 6 Ma a simple orthogonal extensional regime. Gastil and Krummenacher (1977), as well as Gastil *et al.*(1999), by means of reconnaissance mapping with geochronologic data determined that the timing of extensional faulting along coastal Sonora, between Puerto Lobos and Bahia Kino, occurred between 10-7 Ma but more likely before 9 Ma.

Stock and Hodges (1989) first proposed the 'strain partitioning' model for the Pacific-North America plate boundary. The model was supported by estimations of the timing and direction of extensional structures during proto-Gulf time, along with estimations of the direction and amount of Pacific-North America plate motion throughout Miocene time. Neuhaus (1989) studied volcanic rocks in Isla Tiburón with ages between 19 and 15 Ma that were tilted between about 13 and 11 Ma. Based on refined geochronology, additional structural observations, and paleomagnetic data, Oskin *et al*. (2001), as well as Oskin and Stock (2003a), proposed that dextral motion of Baja California was accommodated by faults within the gulf between about 6-7 Ma and the present. Bennett (2013), used paleomagnetic, geochronological and structural data to conclude that the extension in coastal Sonora commenced between 11.5 Ma and 7 Ma**.**

Dextral slip oriented parallel to the Gulf of California (roughly NNW) in the coast of Sonora is inferred from the geometry of the Rancho Nuevo semicircular structure. The geometry is consistent with a very large-scale, *en-echelon*, brittle-ductile shear zone, and this geometry is supported by deformation recorded by AMS fabric and paleomagnetically determined clockwise rotation of about 40º; the model is illustrated in Figure 9. Rhyolite dikes and domes emplaced along sigmoidal fractures in the RNSS are hyperalcaline (Vidal Solano *et al*., 2007).They are related to extension, and their crystallization age is ~13 Ma, and they are

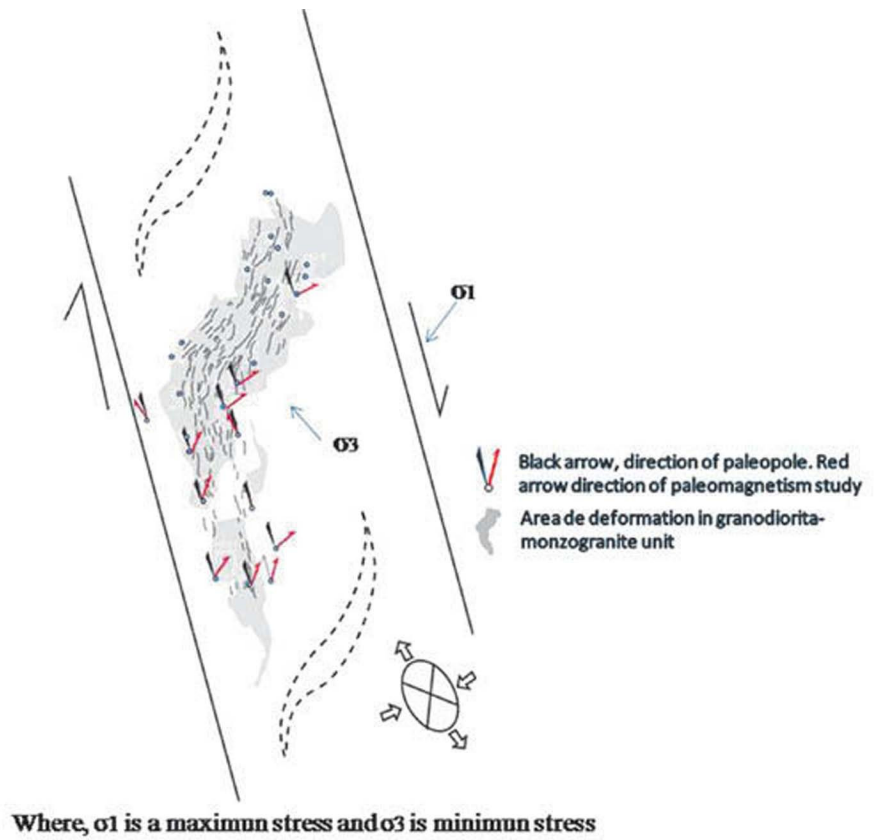

Figure 9. Schematic model of a right-lateral, brittle-ductile, en-echelon pattern of fractures developed in the Rancho Nuevo granitoids and filled by Miocene hyperalkaline dikes. Also indicate the gash fractures formed as extensional fractures that are perpendicular to the minimum compressive stress, Where, σ1 is a maximun stress and σ3 is minimun stress.

discordantly covered by the tuff of San Felipe dated at 12.5 Ma by Vidal Solano *et al.* (2007) and Stock *et al.* (1999).

Our findings suggest that deformation of Cretaceous plutonic rocks at Rancho Nuevo is driven by transtensional shearing along dextral strike-slip faults north and south of the structure, such as the Sacrificio, Infiernillo, and Kino bay faults (Bennett and Oskin, 2007); these faults are most likely related to transtensional motion of Baja California peninsula, and thus the Pacific plate. Some authors (e.g., Oskin and Stock, 2003a,b; Bennett, 2009; and Darin *et al*., 2012) have proposed that right-lateral slip of the peninsula is limited to 7-0 Ma, based on studies of the Miocene volcanic sequence of coastal Sonora. Nonetheless, in this study we recognized the emplacement of hyperalkaline dikes with crystallization ages of ~13 Ma, in plutonic rocks defining an *en-echelon* dextral geometry. The structural observations, such as the presence of striations, crushed plagioclase at microscopic scale, and the magnetic fabric are consistent with a brittle-ductile setting. The deformation is dated at about 13 Ma based on the overlap relationship between tuff San Felipe and rhyolite dikes. Magnetic anisotropy is also consistent with ENE flattening linked to NNE right-lateral shear. We notice that the prolate AMS fabrics at the extremes of the RNSS are also consistent with elongation caused by right-lateral shear. The most convincing evidence of dextral slip and transtensional shearing in late Middle Miocene time is provided, however, by the clockwise rotation observed in the central and southern part of the Rancho Nuevo sigmoid structure. This transtensional deformation is thus related to North America-Pacific plate motion early during the capture of the Baja California Peninsula by the Pacific Plate. may record similar deformation. They include a rhomboidal structure at playa San Bartolo, 27 km to the southwest of Sierra Rancho Nuevo, and a series of dikes located 30 km to the north of the of it, these dikes have a length of the 17 km oriented NNW, suggesting strong structural control by Miocene faults.

Conclusions

The semi-circular Rancho Nuevo structure is a structural dome exposing a Late Cretaceous Plutonic suite partially covered by the ~12.5 Ma tuff of San Felipe. The core of the structure includes granodiorite-monzogranite, monzogranite, quartz-feldespathic porphyry, and granite rich in aplitic dikes and pegmatites. This suite has crystallization age between about 71 and 68 Ma. The plutonic suite is intruded by ~13 Ma (U-Pb zircon) Miocene dikes and disconformably covered by Miocene volcanic rocks.

A sigmoidal fracture pattern affected the plutonic rocks of the RNSS, and it is best developed in the granodiorite-monzogranite body. The fractures were filled by Miocene hyperalkaline dikes, defining an *en-echelon*, brittle-ductile, dextral shear indicator of kilometric scale. Magnetic anisotropy in the plutonic rocks shows a foliation that commonly follows the strike of the dikes, and thus records post-emplacement crystal plastic deformation. In thin section, this deformation is observed as crushed plagioclase grains, undulatory extinction in quartz, and kink-bands. Magnetic fabric suggests elongation to the NNW-ESE, and NW-SE to NE-SW flattening.

The characteristic magnetization in granodiorite of the RNSS is to the southwest and moderately steep negative, indicating (when compared to the expected reference direction) ~40º horizontal rotation about a vertical axis. Rotation is unlikely to have occurred as a simple rigid block. Instead, paleomagnetic data suggest internal deformation of the structure within a zone of dominant right-lateral strain. Therefore, we propose that NNW trending right-lateral faults bound the Rancho Nuevo crystalline block and were active during emplacement of *ca*. 13 Ma hyperalkaline dikes in the RNSS. This suggests that strain was localized. We also propose that these faults accommodated part of the NW motion of Baja California peninsula during the proto-Gulf event.

Acknowledgements

We thank CONACYT who supported the research of D.García and R. Molina with CB grant 12982. We also thank Thierry Calmus, José Luis Rodriguez C, and Sergio Salgado S. for their comments and support. Alexander Iriondo provided direction and support in U-Pb determinations at Centro de Geociencias, Juriquilla. We also thank Aimée Orci Romero for thin section preparation, Pablo Peñaflor Escárcega for help in sample preparation, and Jesús Vidal Solano for valuable comments to previous version of this manuscript and discussion of hyperalcaline magmas. We thank Mr. Pilo Galáz y Mr. Miguel Robles for access to their properties, as well as Gonzalo Ibarra for his assistance in the field. We thank Dr. Garcia y Barragán, for his detailed review of the paper. The comments of K. Busby and treewo anonymous reviewers served to improve this article and are greatly appreciated.

References

Ávila–Ángulo R., 1987, Consideraciones geológicas y estratigráficas de la porción NW de Hermosillo: México: Hermosillo, Son., Universidad de Sonora, Departamento de Geología, Tesis de licenciatura, 78 p.

Atwater T., 1970, Implications of plate tectonics for the Cenozoic evolution of western North America: *Geological Society of America Bulletin,* 81, p. 3513–3536.

Atwater T., Stock J.M., 1998, Pacific–North America plate tectonics of the Neogene southwestern United States: An update: *International Geology Review,* 40, p. 375–402.

Atwater T., 1989, Plate tectonic, history of northeastern Pacific and western North America: In Wintered E. L., Hussong, D. M, and Decker R. W., (Eds.) The eastern Pacific ocean and Hawaii: Geological Society of America, *The geology of North America,* N, p. 21-72.

Bennett S.E.K., Oskin M., 2007, Transition from Proto-Gulf Extension to Transtension. Coastal Sonora, México: *Eos Transactions American Geophysical Union*, 88; P.Abstract S31A-10.

Bennett S.E.K., 2009, Transtensional Rifting in the late Proto-Gulf of California Near Bahia Kino, Sonora Mexico. Thesis Master Sciences, Department of Geological Sciences, North Caroline University at Chapel Hill, 122 p.

Bennett S.E.K., Oskin M.E., Iriondo A., 2013, Transtensional rifting in the proto–Gulf of California near Bahía Kino, Sonora, México. *Geological Society of America Bulletin.*

Besse J., Courtillot V., 2002, Apparent and true polar wanderand the geometry of the geomagnetic field over the last200 Myr. *Journal of Geophysical Research-Solid Earth,* 107, B11.

Borradaile, G.J. 1988, *Magnetic Susceptibility, petrofabrics and strain, Tectonophysics,* v. 156,p.1-20.

Borradaile G.J., Henry B., 1997, Tectonic application of magnetic susceptibility and its anisotropy. *Earths Sci.* Review 4, 49-93.

Damon P.E., Shafiqullah M., Clark K.F., 1981, Evolución de los arcos magmáticos en México y su relación con la metalogenesis, *Revista Mexicana de Ciencias Geológicas*, 5, 223-238.

Darin M.H., Dorsey, R. J., Bennett, S.E.K., Oskin, M. and Iriondo, A., 2012, Late Miocene extension in the Sierra Bacha, coastal Sonora, Mexico: implications for the kinematic evolution of the Proto-Gulf of California. Cordilleran Section - 108th GSA *Annual Meeting Abstracts with Programs* (29–31), Juriquilla Querétaro.

Ellwood B.B., Wenner D.B., 1981, Correlation of magnetitic susceptibility with18O/16O data in late orogenic granites of the southern Appalachian Piedmont, *Earth and Planetary Science Letters,* 54, 200-202.

Fletcher J.M., Grove M., Kimbrough D., Lovera O., Gehrels G.E., 2007, Ridge-trench interactions and the Neogene tectonic evolution of the Magdalena shelf and southern Gulf of California: In sigthts from the detrital zircon U-Pb ages from the Magdalena fan adjacent areas; *Geological Society of America, Bulletin,* 119, 1313-1336.

Gans P.B., 1997, Large-magnitude Oligo-Miocene extension in southern Sonora: *Implications for the tectonic evolution of northwest Mexico, Tectonics,* 16, 338-408.

Gastil G., Krummenacher D., 1974, Reconnaissance geology map of coastal Sonora between Puerto Lobos and Bahia Kino, *Geological Society of America* Map and Chart Series MC-16 scala 1:150,000.

Gastil G., Krummenacher D., 1977, Reconnaissance geology of coastal Sonora between Puerto Lobos and Bahia Kino: *Geological Society of America Bulletin,* 88, 189–198.

Gastil G.R., Neuhaus J., Cassidy M., Smith J.T, Ingle J.C., Krummenancher D., 1999, Geology and paleontology of southwestern Isla Tiburon Sonora Mexico. *Revista Mexicana de Ciencias Geologicas,* 16 p. 1-34.

Gehrels G, Valencia V., Pullen A., 2006, Detrital zircon Geochronology by Laser Ablation Multicollector, ICPMS at Arizona LaserChron Center in Olszewszki.T.D. (ed).

Geochronology emerging opportunities: Paleontological Society papers, 12, 67-76.

Hausback B.P., 1984, Cenozoic volcanic and tectonic evolution of Baja California Sur, Mexico, in Frizell, V. A; Jr; ed; *Geology of the Baja California Peninsula,* Volume 39; los Angeles, California, Pacific Section of the Economic Paleontologists and Mineralogist. P. 219-236.

Karig D.E., Jensky W., 1972, The proto-Gulf of California, *Earth and Planetary Science Letters*, 17, p. 169–174.

Kirschvink J., 1980, The least-squares line and plane and the analysis of palaeomagnetic data, *Geophys. J. Int.*, 62, 699-718.

Lewis C.J., 1996, Stratigraphy and geochronology of Miocene and Pliocene volcanic rocks in the Sierra San Fermin and Southern Sierra San Felipe, Baja California, Mexico, *Geofísica Internacional*, 36, 1-31.

McDowell F.W., Roldán-Quintana J.J., Amaya-Martínez R., 1997, Interrelationship of sedimentary and volcanic deposits associated with Tertiary extension in Sonora, Mexico,*Geological Society of America Bulletin*, 109, p. 1349–1360.

Neuhaus J.R., 1989, Volcanic and non marine stratigraphy of southwest Isla Tiburón, Gulf of California, Thesis: San Diego California, San Diego California State University, 170 p.

Nourse J.A., Anderson T.H., Silver L.T., 1994, Tertiary metamorphic core complexes in Sonora, northwestern Mexico:Tectonics, 13, p. 1161–1182.

Oskin M., Stock J., Martin-Barajas A., 2001, Rapid localization of Pacific-North America plate motions in the Gulf of California,29, p. 459-462.

Oskin M., 2002, Tectonic evolution of the northern Gulf of California, Mexico deduce from conjugated rifted margins of the Upper Delfin Basin (Ph. Thesis): Pasadena California Institute of Technology, 481 P.

Oskin M., Stock J.M, 2003a, Pacific-North America plate motion and opening of the Upper Delfin basin, northern Gulf of California: *Geological Society of America Bulletin,* 115, p. 1173-1190.

Oskin M., Stock J., 2003b, Cenozoic volcanism and tectonics of the continental margins of the Delfin basin, northern Gulf of California, Mexico, Johnson, S. *et al*., eds. Tectonic Evolution of Northwestern México and Southwestern USA: Boulder, Colorado, *Geological Society of America Special Paper,* 374, p. 421-438.

Poole F.G., 1993, Ordovician eugeoclinal rocks in Turner Island, in the Gulf of California, Sonora, Mexico. Universidad Autónoma de México, Instituto de Geología and Universidad de Sonora, departamento de Geología. Simposio de la geología de Sonora y areas adyacentes 3rd, Hermosillo, Sonora; México. Resumenes. P. 103.

Poole F.G., William J. Jr., Madrid R.J., Amaya-Martinez R., 2005, Tectonic synthesis of the Ouachita-Marathon-Sonora orogenic margin of southern Laurentia: Stratigraphic and structural implications for timing of deformational events and plate-tectonic model.

Ramos-Velázquez E., Calmus T., Valencia V., Iriondo A., Valencia-Moreno M., Bellon H., 2008, U-Pb and 40Ar/39Ar geochronology of the Coastal Sonora Batholith: new insights on Laramide continental arc magmatism. *Revista Mexicana de Ciencias Geológicas,* 25, 2 p. 314-333.

Seilers C., Fletcher J.M, Quigley M.C, Gleadow A.J, Kohn. B. P. 2010. Neogene structural evolution of the Sierra San Felipe, Baja California: *Evidence for proto-gulf transtension in the Gulf Extensional Province?Tectonophysics,* 488, 1–4, 5 June 2010, Pages 87–109

Servicio Geológico Mexicano, 2008, Carta Geológica Minera Estado de Sonora, 1:500,000., Boulevard Felipe Ángeles Km. 93.5-4, Col. Venta Prieta, C.P. 42080 Pachuca, Hidalgo.

Solari L.A., Gómez-Tuena A., Bernal J.P., Pérez-Arvizu O., Tanner M., 2010, U-Pb Zircon Geochronology with an Integrated LA-ICP-MS Microanalytical Workstation, Achievements in Precision and Accuracy Geostandards and Geoanalytical Research, 34, 5-18.

Stewart J.H., 1988,Latest Proterozoic and Paleozoic southern margin of North America and the accretion of Mexico, *Geology*, 16 P. 186-189.

Stock J.M., 1989, Sequence and geochronology of Miocene rocks adjacent to the main Gulf escarpment: Southern Valle Chico, Baja California Norte, Mexico: *Geofísica Internacional,* 28, 851-896.

Stock J.M., Hodges K.V., 1989, Pre-Pliocene Extension around the Gulf of California and the transfer of Baja California to the Pacific: Tectonics, 8, 99-115. *Relative to the Farallon, Kula, and Pacific plates: Tectonics*, 6, p. 1339-1384.

Stock J.M., Molnar P., 1988, Uncertainties and implications of the Late Cretaceous and Tertiary position of North America.

Streickeisen A.L., 1976, Classification of the common igneous rocks by means of their chemical composition: a provisional attempt. Neues Jahrbuch fur Mineralogie, Monatshefte, 1976, H.l, 1-15.

Valencia-Moreno J. Ruiz, Ochoa-Landín L., Martínez-Serrano R., Vargas-Navarro P., 2003, Geochemistry of the Coastal batholith, Northwestern México**.** *Canadian Journal of Earth Sciences,* 40, 819-831.

Vega-Granillo R., Calmus T., 2003, Mazatán metamorphic core complex (Sonora, Mexico) Structures along the detachment fault and its exhumation evolution: *Journal of South American Earth Sciences,* 16, 4, p. 193–204.

Vernon R.H., 1975, Deformation and recrystallization of a plagioclase grain. *American Mineralogist*, 60, 884-888.

Vidal-Solano J., Paz Moreno F.A., Demant A., López-Martínez M., 2007, Ignimbritas hiperalcalinas del Mioceno medio en Sonora Central—Revaluación de la estratigrafía y significa do del volcanismo terciario: *Revista Mexicana de Ciencias Geológicas,* 24, p. 47–67.

Wong M.S., Gans P.B., 2008, Geologic, structural, and thermochronologic constraints on the tectonic evolution of the Sierra Mazatán core complex, Sonora, Mexico: *New insights into metamorphic core complex formation. Tectonics*, 27, 4, TC4013.

Umhoefer P.J., Dorsey R.J., Sillsey S., Mayer L., Renne P., 2001, Stratigraphy and geochronology of the Comondú Group near Loreto, Baja California sur, Mexico, *Sedimentary Geology*, 144, 125-147.

Appendix 1. Table of Percentages of quartz, feldspar and plagioclase, and classification of the major intrusive units in RNSS. Nomenclature: Unidad Gd-Mzgr = granodiorite-monzogranite, UnidadGrG = monzogranite GrC = granite rich in quartz, aplitic dikes and pegmatites. And location in UTM WGS84, Zone 12.

Sample name	Unit	Coord E	Coord N	Quartz%	K-Feld-spar%	Plagioclase %	Classification
T 23	Gd-Mzgr	419178	3249104	17.34	25.16	57.50	Gd
Oeste	Gd-Mzgr	417124	3250151	17.64	25.40	56.94	Gd
PdA	Gd-Mzgr	421360	3252144	16.55	27.35	56.10	Gd
T 35	Gd-Mzgr	422750	3255818	14.69	39.30	46.01	Gd
T 30	Gd-Mzgr	416533	3253342	29.78	23.27	46.93	Gd
T 33a	Gd-Mzgr	421297	3253474	16.28	41.20	42.50	Gd
T 212	Gd-Mzgr	418797	3253613	27.52	27.52	49.94	Gd-Mzgr
T 30 A	Gd-Mzgr	417126	3252972	13.78	35.42	41.88	Mzgr
NWGA	Gd-Mzgr	427007	3259018	31.11	28.90	39.95	Mzgr
T 209	Gd-Mzgr	418206	3253914	31.64	33.67	34.68	Mzgr
T 21 2 GB	Gd-Mzgr	418853	3253558	34.70	40.78	24.51	Mzgr
T 214	Gd-Mzgr	418511	3253372	25.28	49.66	27.04	Mzgr
TR 12 36	Gd-Mzgr	424988	3248395	26.86	47.71	25.42	Mzgr
T 4	GrG	419832	3243410	28.23	39.30	32.47	Mzgr
T 1	GrG	420614	3243460	38.69	39.43	21.88	Mzgr
T 29	Grc	416289	3252218	13.78	61.87	24.40	Grcz

Appendix 2. Tables a,b,c,d,e, U-Pb isotopic relations of zircon analyzes in major RNSS units.

Tabla 2a

				CORRECTED RATIOS										CORRECTED AGES (Ma)								
	U* (ppm)	Th* (ppm)	Th/U	$^{207}Pb/^{206}Pb$	±1s	$^{207}Pb/^{235}U$	±1s	$^{206}Pb/^{238}U$	±1s	$^{208}Pb/^{232}Th$	±1s	Rho	% disc	$^{206}Pb/^{238}U$	±1s	$^{207}Pb/^{235}U$	±1s	$^{207}Pb/^{206}Pb$	±1s	$^{208}Pb/^{232}Th$	±1s	Best age (Ma) ± 1s
Sample **T-205**	(Andesite)	Mount DAVID-1 (November 2012)																				
T205_**10**	157	71	0.39	0.0640	0.0063	0.1024	0.0105	0.0116	0.00023	0.0036	0.00008	0.220	25	74.0	1.0	99.0	10.0	743	202	72.0	2.0	74.0 ± 1.0
T205_**2**	151	97	0.55	0.0631	0.0057	0.1062	0.0097	0.0122	0.00019	0.0041	0.00016	0.170	24	78.0	1.0	102.0	9.0	712	186	82.0	3.0	78.0 ± 1.0
T205_**3**	194	108	0.48	0.0678	0.0053	0.1126	0.0089	0.0122	0.00018	0.0039	0.00016	0.190	28	78.0	1.0	108.0	8.0	864	157	79.0	3.0	78.0 ± 1.0
T205_**12**	331	205	0.53	0.0668	0.0066	0.1123	0.0113	0.0122	0.00022	0.0036	0.00019	0.180	28	78.0	1.0	108.0	10.0	831	202	72.0	4.0	78.0 ± 1.0
T205_**13**	125	60	0.41	0.0692	0.0082	0.1156	0.0138	0.0121	0.00018	0.0037	0.00009	0.120	30	78.0	1.0	111.0	13.0	903	241	74.0	2.0	78.0 ± 1.0
T205_**1**	632	483	0.66	0.0573	0.0037	0.0978	0.0064	0.0123	0.00016	0.0038	0.00010	0.190	17	79.0	1.0	95.0	6.0	504	135	76.0	2.0	79.0 ± 1.0
T205_**7**	248	182	0.63	0.0663	0.0076	0.1135	0.0134	0.0124	0.00022	0.0038	0.00009	0.140	27	80.0	1.0	109.0	12.0	816	237	76.0	2.0	80.0 ± 1.0
T205_**9**	216	173	0.69	0.0570	0.0037	0.0984	0.0065	0.0126	0.00016	0.0041	0.00013	0.200	16	80.0	1.0	95.0	6.0	492	138	83.0	3.0	80.0 ± 1.0
T205_**19**	195	92	0.41	0.0636	0.0057	0.1106	0.0102	0.0126	0.00016	0.0039	0.00007	0.150	24	80.8	1.0	106.0	9.0	729	186	78.0	1.0	80.8 ± 1.0
T205_**4**	113	76	0.58	0.0741	0.0096	0.1300	0.0171	0.0126	0.00021	0.0042	0.00026	0.130	35	81.0	1.0	124.0	15.0	1045	262	84.0	5.0	81.0 ± 1.0
T205_**16**	193	128	0.57	0.0638	0.0051	0.1118	0.0095	0.0127	0.00018	0.0039	0.00006	0.210	25	81.0	1.0	108.0	9.0	733	164	79.0	1.0	81.0 ± 1.0
T205_**18**	305	248	0.70	0.0789	0.0079	0.1408	0.0143	0.0130	0.00025	0.0041	0.00014	0.180	38	83.0	2.0	134.0	13.0	1168	194	83.0	3.0	83.0 ± 2.0
T205_**11**	162	65	0.34	0.0631	0.0040	0.1137	0.0075	0.0132	0.00018	0.0045	0.00027	0.210	23	84.0	1.0	109.0	7.0	711	131	90.0	5.0	84.0 ± 1.0
T205_**14**	271	141	0.45	0.0639	0.0042	0.1254	0.0083	0.0142	0.00017	0.0045	0.00018	0.190	24	91.0	1.0	120.0	7.0	738	132	90.0	4.0	91.0 ± 1.0
																					Weighted $^{206}Pb/^{238}U$ mean age =	79.5 ± 1.0

Tabla 2b

	U* (ppm)	Th* (ppm)	Th/U	$^{207}Pb/^{206}Pb$	±1s	$^{207}Pb/^{235}U$	±1s	$^{206}Pb/^{238}U$	±1s	$^{208}Pb/^{232}Th$	±1s	Rho	% disc	$^{206}Pb/^{238}U$	±1s	$^{207}Pb/^{235}U$	±1s	$^{207}Pb/^{206}Pb$	±1s	$^{208}Pb/^{232}Th$	±1s	Best age (Ma) ± 1s
Sample **TR-12-46**	(San Felipe Tuff)	Mount DAVID-1 (November 2012)																				
TR1246_**13**	467	227	0.42	0.0750	0.0122	0.0206	0.0034	0.0020	0.00003	0.0006	0.00001	0.110	39	12.8	0.2	21.0	3.0	1068	335	12.1	0.3	12.8 ± 0.2
TR1246_**1**	537	419	0.67	0.0842	0.0118	0.0230	0.0033	0.0020	0.00004	0.0007	0.00004	0.160	44	12.9	0.3	23.0	3.0	1296	282	13.5	0.8	12.9 ± 0.3
TR1246_**18**	614	402	0.56	0.0741	0.0108	0.0209	0.0032	0.0020	0.00005	0.0006	0.00002	0.180	38	13.1	0.4	21.0	3.0	1045	304	12.4	0.4	13.1 ± 0.4
TR1246_**15**	390	179	0.39	0.0853	0.0151	0.0247	0.0045	0.0021	0.00005	0.0006	0.00002	0.160	46	13.5	0.3	25.0	4.0	1322	359	12.6	0.4	13.5 ± 0.3
TR1246_**20**	356	160	0.38	0.0929	0.0127	0.0271	0.0038	0.0021	0.00003	0.0006	0.00001	0.160	50	13.6	0.2	27.0	4.0	1485	267	12.6	0.2	13.6 ± 0.2
TR1246_**10**	345	149	0.37	0.0834	0.0196	0.0244	0.0059	0.0021	0.00008	0.0006	0.00004	0.160	43	13.7	0.5	24.0	6.0	1277	482	12.8	0.9	13.7 ± 0.5
TR1246_**16**	258	101	0.34	0.1072	0.0183	0.0316	0.0056	0.0021	0.00006	0.0006	0.00002	0.190	57	13.8	0.4	32.0	5.0	1753	330	12.5	0.4	13.8 ± 0.4
TR1246_**19**	636	359	0.48	0.0937	0.0088	0.0277	0.0027	0.0022	0.00006	0.0007	0.00006	0.280	51	13.8	0.4	28.0	3.0	1502	180	15.0	1.0	13.8 ± 0.4
TR1246_**4**	345	177	0.44	0.0949	0.0122	0.0283	0.0038	0.0022	0.00005	0.0006	0.00002	0.210	50	13.9	0.3	28.0	4.0	1526	249	12.8	0.3	13.9 ± 0.3
TR1246_**3**	306	137	0.39	0.0674	0.0130	0.0201	0.0041	0.0022	0.00007	0.0007	0.00004	0.210	30	14.0	0.5	20.0	4.0	850	402	13.3	0.9	14.0 ± 0.5
																					Weighted $^{206}Pb/^{238}U$ mean age =	13.38 ± 0.32

Tabla 2c

Sample T 92

				Isotope ratios							Apparent ages (Ma)							
Analysis Sample	U (ppm)	206Pb/204Pb	U/Th	206Pb*/207Pb*	± (%)	207Pb*/235U*	± (%)	206Pb*/238U	± (%)	error corr.	206Pb*/238U*	± (Ma)	207Pb*/235U	± (Ma)	206Pb*/207Pb*	± (Ma)	Best age (Ma)	± (Ma)
T 92																		
T-92-4C	138	4136	1.3	20.6184	21.0	0.0703	21.6	0.0105	5.2	0.24	67.4	3.5	69.0	14.4	123.7	498.2	67.4	3.5
T-92-5C	107	5239	1.1	19.9224	21.9	0.0737	22.1	0.0107	3.3	0.15	68.3	2.3	72.2	15.4	204.0	513.5	68.3	2.3
T-92-1C	148	6899	0.9	20.2710	16.9	0.0727	17.7	0.0107	5.1	0.29	68.5	3.4	71.2	12.1	163.6	397.9	68.5	3.4
T-92-2	119	8051	1.3	28.4349	36.2	0.0522	36.9	0.0108	7.3	0.20	69.0	5.0	51.6	18.6	-695.3	1030.9	69.0	5.0
T-92-11C	171	7126	1.3	22.1416	24.4	0.0673	24.7	0.0108	4.4	0.18	69.3	3.0	66.1	15.8	-46.8	599.9	69.3	3.0
T-92-22	756	57076	1.4	21.0308	3.6	0.0711	3.9	0.0108	1.2	0.32	69.5	0.9	69.7	2.6	76.9	86.7	69.5	0.9
~~T-92-26~~	~~71~~	~~2329~~	~~1.9~~	~~-3.6181~~	~~2791.0~~	~~-0.4137~~	~~2791.0~~	~~0.0109~~	~~5.2~~	~~0.00~~	~~69.6~~	~~3.6~~	~~-542.1~~	~~#NUM!~~	~~NA~~	~~NA~~	~~69.6~~	~~3.6~~
T-92-6	136	3741	2.0	23.7501	21.1	0.0631	21.5	0.0109	4.0	0.19	69.7	2.8	62.1	12.9	-220.2	535.3	69.7	2.8
T-92-1R	193	17252	0.9	19.6781	28.9	0.0764	29.2	0.0109	3.8	0.13	70.0	2.6	74.8	21.0	232.6	680.3	70.0	2.6
T-92-5R	369	33517	1.6	20.5516	5.2	0.0732	5.4	0.0109	1.5	0.28	70.0	1.1	71.7	3.7	131.4	121.9	70.0	1.1
T-92-19	134	7268	1.7	21.8638	21.9	0.0689	22.1	0.0109	2.7	0.12	70.0	1.9	67.6	14.5	-16.2	536.2	70.0	1.9
T-92-12F	255	7186	2.3	22.5509	11.0	0.0670	11.3	0.0110	2.4	0.21	70.3	1.7	65.9	7.2	-91.5	270.7	70.3	1.7
T-92-18	330	21575	1.5	21.7280	8.7	0.0696	8.8	0.0110	1.5	0.17	70.4	1.1	68.4	5.8	-1.1	210.4	70.4	1.1
T-92-7	101	7481	1.6	16.1132	13.1	0.0946	13.8	0.0111	4.3	0.31	70.9	3.0	91.8	12.1	676.2	282.1	70.9	3.0
T-92-24	131	3652	1.7	28.6960	52.7	0.0531	52.9	0.0111	3.8	0.07	70.9	2.7	52.6	27.1	-720.7	1565.1	70.9	2.7
T-92-3	115	4210	1.5	24.1043	27.7	0.0633	28.2	0.0111	5.2	0.18	71.0	3.6	62.3	17.0	-257.6	713.1	71.0	3.6
T-92-4R	799	25668	1.6	21.0825	3.7	0.0728	3.9	0.0111	1.2	0.32	71.3	0.9	71.3	2.7	71.1	87.7	71.3	0.9
T-92-16	207	6106	2.0	24.1835	25.7	0.0635	25.9	0.0111	3.2	0.12	71.4	2.3	62.5	15.7	-265.9	660.7	71.4	2.3
T-92-14	156	4285	2.0	21.4076	9.2	0.0717	9.5	0.0111	2.2	0.23	71.4	1.5	70.4	6.4	34.5	221.5	71.4	1.5
T-92-17	86	3623	1.6	32.9897	66.2	0.0466	66.5	0.0111	6.5	0.10	71.4	4.6	46.2	30.1	-1127.2	2240.3	71.4	4.6
T-92-15	200	6203	1.6	19.8637	9.8	0.0773	10.9	0.0111	4.9	0.45	71.4	3.5	75.6	8.0	210.9	227.1	71.4	3.5
T-92-8	369	5988	1.9	19.7826	8.0	0.0781	8.3	0.0112	2.2	0.27	71.8	1.6	76.3	6.1	220.3	184.4	71.8	1.6
T-92-23	129	6106	1.8	21.0667	16.7	0.0734	17.3	0.0112	4.6	0.27	71.9	3.3	72.0	12.0	72.8	399.8	71.9	3.3
T-92-20	201	8003	1.9	19.6515	21.1	0.0793	21.2	0.0113	1.8	0.08	72.5	1.3	77.5	15.8	235.7	491.5	72.5	1.3
T-92-13	190	8139	2.0	22.6545	18.0	0.0692	18.5	0.0114	4.5	0.24	72.9	3.3	68.0	12.2	-102.8	444.9	72.9	3.3
T-92-21	461	19982	1.6	20.7453	9.0	0.0758	9.2	0.0114	2.0	0.22	73.1	1.5	74.2	6.6	109.3	212.8	73.1	1.5
T-92-10	416	9570	1.9	20.2337	8.8	0.0784	9.0	0.0115	1.8	0.20	73.7	1.3	76.6	6.6	167.9	205.6	73.7	1.3
T-92-9	663	24410	8.8	20.7664	4.9	0.0790	5.5	0.0119	2.5	0.46	76.3	1.9	77.2	4.1	106.9	116.5	76.3	1.9

Final Age = 71.1 ± 1.1 Ma

Tabla d

				Isotope ratios								Apparent ages (Ma)					
Analysis	U (ppm)	206Pb 204Pb	U/Th	206Pb* 207Pb*	± (%)	207Pb* 235U*	± (%)	206Pb* 238U	± (%)	error corr.	206Pb 238U*	± (Ma)	207Pb* 235U	± (Ma)	206Pb* 207Pb*	± (Ma)	Best age (Ma)	± (Ma)
Sample T91																		
T-91-21	643	30834	2.0	20.7246	3.1	0.0676	4.2	0.0102	2.9	0.69	65.2	1.9	66.4	2.7	111.7	72.7	65.2	1.9
T-91-7	300	24051	2.0	21.3900	6.9	0.0655	7.6	0.0102	3.1	0.41	65.2	2.0	64.4	4.7	36.5	165.1	65.2	2.0
T-91-8(	189	13018	1.3	22.1308	9.1	0.0635	9.4	0.0102	2.6	0.27	65.4	1.7	62.5	5.7	-45.6	221.0	65.4	1.7
T-91-13	916	87854	1.6	20.7838	2.2	0.0685	3.9	0.0103	3.3	0.84	66.2	2.2	67.2	2.6	104.9	51.0	66.2	2.2
T-91-19	1508	41523	1.7	20.7165	1.6	0.0689	3.6	0.0104	3.3	0.90	66.4	2.2	67.7	2.4	112.6	36.8	66.4	2.2
T-91-9	773	8444	1.7	20.2192	6.5	0.0707	6.5	0.0104	0.7	0.10	66.4	0.4	69.3	4.4	169.6	151.4	66.4	0.4
T-91-25	219	3919	1.8	19.5131	9.3	0.0739	9.6	0.0105	2.5	0.26	67.0	1.7	72.4	6.7	252.0	214.3	67.0	1.7
T-91-12	1204	141473	1.7	20.7729	1.1	0.0698	1.4	0.0105	0.9	0.60	67.4	0.6	68.5	0.9	106.1	27.0	67.4	0.6
T-91-6F	526	4050	1.5	20.1310	7.0	0.0726	8.5	0.0106	4.8	0.57	67.9	3.3	71.1	5.9	173.8	164.1	67.9	3.3
T-91-2	711	50504	1.6	21.3532	3.0	0.0685	3.2	0.0106	0.9	0.28	68.0	0.6	67.3	2.1	40.7	72.8	68.0	0.6
T-91-12	286	11670	1.5	20.6440	4.6	0.0711	5.0	0.0106	2.1	0.41	68.3	1.4	69.8	3.4	120.8	107.9	68.3	1.4
T-91-23	712	33895	1.8	21.0038	2.0	0.0699	2.2	0.0106	0.9	0.40	68.3	0.6	68.6	1.4	79.3	46.9	68.3	0.6
T-91-6(	155	8885	1.5	20.6822	17.0	0.0713	17.6	0.0107	4.6	0.26	68.5	3.1	69.9	11.9	116.5	404.0	68.5	3.1
T-91-4	122	5499	1.5	27.0084	18.6	0.0546	18.9	0.0107	3.5	0.19	68.5	2.4	53.9	9.9	-554.7	503.0	68.5	2.4
T-91-10	130	8138	1.2	21.2941	11.9	0.0692	12.4	0.0107	3.5	0.29	68.6	2.4	68.0	8.1	47.3	284.3	68.6	2.4
T-91-1	74	3963	1.9	22.4245	32.2	0.0658	32.6	0.0107	4.9	0.15	68.7	3.3	64.7	20.5	-77.8	806.7	68.7	3.3
T-91-11	672	13321	1.9	21.0900	2.8	0.0702	3.0	0.0107	1.0	0.34	68.9	0.7	68.9	2.0	70.2	66.8	68.9	0.7
T-91-18	525	38327	2.1	21.3412	3.2	0.0696	3.4	0.0108	1.2	0.34	69.1	0.8	68.3	2.3	42.0	76.6	69.1	0.8
T-91-17	188	9126	1.9	20.2595	9.1	0.0735	9.4	0.0108	2.3	0.25	69.2	1.6	72.0	6.5	164.9	213.2	69.2	1.6
T-91-2(	649	33040	1.7	20.9742	3.0	0.0713	3.2	0.0108	1.1	0.35	69.6	0.8	69.9	2.1	83.3	70.6	69.6	0.8
T-91-19	117	4811	1.5	26.3594	26.5	0.0568	26.7	0.0109	3.4	0.13	69.6	2.3	56.1	14.6	-489.6	714.9	69.6	2.3
T-91-10	629	33002	2.0	20.8778	4.5	0.0720	7.2	0.0109	5.6	0.78	69.9	3.9	70.5	4.9	94.2	106.0	69.9	3.9
T-91-2(	236	9814	1.6	21.5593	5.5	0.0708	5.9	0.0111	2.1	0.35	71.0	1.5	69.5	4.0	17.6	133.4	71.0	1.5
T-91-15	130	12539	2.1	20.7556	8.1	0.0737	8.7	0.0111	3.0	0.35	71.1	2.2	72.2	6.0	108.1	191.5	71.1	2.2
~~T-91-22~~	~~465~~	~~8086~~	~~1.9~~	~~20.9001~~	~~4.8~~	~~0.0739~~	~~5.1~~	~~0.0112~~	~~1.7~~	~~0.33~~	~~71.8~~	~~1.2~~	~~72.4~~	~~3.6~~	~~81.7~~	~~113.9~~	~~71.8~~	~~1.2~~
~~T-91-16~~	~~121~~	~~12949~~	~~2.3~~	~~24.2348~~	~~20.8~~	~~0.0638~~	~~21.0~~	~~0.0112~~	~~3.2~~	~~0.15~~	~~71.9~~	~~2.3~~	~~62.8~~	~~12.8~~	~~-271.3~~	~~532.3~~	~~71.9~~	~~2.3~~
~~T-91-25~~	~~319~~	~~17444~~	~~2.2~~	~~20.5678~~	~~4.7~~	~~0.0759~~	~~4.8~~	~~0.0113~~	~~1.2~~	~~0.25~~	~~72.6~~	~~0.9~~	~~74.3~~	~~3.5~~	~~123.5~~	~~110.5~~	~~72.6~~	~~0.9~~
~~T-91-5~~	~~3115~~	~~52862~~	~~1.8~~	~~21.1024~~	~~1.2~~	~~0.0767~~	~~3.2~~	~~0.0117~~	~~3.0~~	~~0.93~~	~~75.2~~	~~2.2~~	~~75.0~~	~~2.3~~	~~68.8~~	~~28.3~~	~~75.2~~	~~2.2~~
~~T-91-5(~~	~~329~~	~~23144~~	~~1.6~~	~~20.3940~~	~~7.0~~	~~0.0831~~	~~7.6~~	~~0.0123~~	~~2.8~~	~~0.36~~	~~78.7~~	~~2.2~~	~~81.1~~	~~5.9~~	~~350.6~~	~~355.0~~	~~78.7~~	~~2.2~~

Final Age = 68±1.0 Ma

Tabla e

				Isotope ratios								Apparent ages (Ma)					
Analysis	U (ppm)	206Pb 204Pb	U/Th	206Pb* 207Pb*	± (%)	207Pb* 235U*	± (%)	206Pb* 238U	± (%)	error corr.	206Pb 238U*	± (Ma)	207Pb* 235U	± (Ma)	206Pb* 207Pb*	± (Ma)	Best age (Ma)	± (Ma)
T83																		
T-83-4(	75	2003	1.5	30.7463	24.8	0.0452	25.3	0.0101	5.3	0.21	64.6	3.4	44.9	11.1	-917.3	729.2	64.6	3.4
T-83-1(	236	10809	1.2	22.4414	15.4	0.0629	15.7	0.0102	3.2	0.20	65.7	2.1	62.0	9.4	-79.6	378.0	65.7	2.1
T-83-17	380	18727	1.6	20.3459	6.2	0.0699	6.8	0.0103	2.7	0.40	66.2	1.8	68.6	4.5	155.0	145.7	66.2	1.8
T-83-1(	230	11534	1.1	20.7611	7.7	0.0688	7.9	0.0104	1.9	0.24	66.4	1.3	67.6	5.2	107.5	181.1	66.4	1.3
T-83-1(	130	5971	1.0	22.4664	24.9	0.0642	26.7	0.0105	9.8	0.37	67.1	6.5	63.2	16.4	-82.3	616.9	67.1	6.5
T-83-2(	1325	29208	2.0	21.3325	3.0	0.0677	3.1	0.0105	0.9	0.30	67.2	0.6	66.5	2.0	42.9	70.6	67.2	0.6
T-83-9(	185	8188	1.2	20.2446	12.4	0.0716	12.9	0.0105	3.7	0.29	67.4	2.5	70.2	8.8	166.6	290.1	67.4	2.5
T-83-5(	1279	53900	3.6	21.4256	3.5	0.0679	4.2	0.0106	2.4	0.56	67.7	1.6	66.7	2.7	32.5	83.0	67.7	1.6
T-83-8(	227	9250	1.0	23.6155	12.2	0.0617	13.0	0.0106	4.5	0.35	67.8	3.0	60.8	7.7	-205.9	306.3	67.8	3.0
T-83-2(	391	18828	1.3	21.4851	3.2	0.0679	3.5	0.0106	1.4	0.40	67.9	1.0	66.7	2.3	25.9	77.8	67.9	1.0
T-83-2(	1536	115724	1.1	21.1968	1.7	0.0691	2.7	0.0106	2.1	0.77	68.1	1.4	67.8	1.8	58.2	40.7	68.1	1.4
T-83-1(	292	25825	1.1	22.3073	12.6	0.0657	12.8	0.0106	2.4	0.19	68.2	1.6	64.6	8.0	-65.0	308.6	68.2	1.6
T-83-4(	355	13260	1.2	22.4428	8.8	0.0656	10.5	0.0107	5.8	0.55	68.4	3.9	64.5	6.6	-79.8	215.7	68.4	3.9
T-83-7(	596	23165	0.8	22.6088	5.9	0.0651	6.3	0.0107	2.3	0.37	68.4	1.6	64.0	3.9	-97.8	145.0	68.4	1.6
T-83-1(	590	38815	2.7	22.2804	7.5	0.0662	8.0	0.0107	3.0	0.37	68.5	2.0	65.0	5.1	-62.0	182.2	68.5	2.0
T-83-2(	1719	69659	4.2	21.0434	3.2	0.0703	3.8	0.0107	2.1	0.55	68.8	1.4	69.0	2.5	75.5	75.1	68.8	1.4
T-83-3(	2023	118540	3.2	21.1849	1.4	0.0700	1.9	0.0108	1.3	0.69	68.9	0.9	68.7	1.3	59.6	33.0	68.9	0.9
T-83-2(	3056	137059	1.2	21.0718	1.2	0.0704	6.5	0.0108	6.4	0.98	69.0	4.4	69.1	4.3	72.3	28.1	69.0	4.4
T-83-1F	335	9642	2.1	21.2334	9.6	0.0701	12.8	0.0108	8.4	0.66	69.2	5.8	68.8	8.5	54.1	230.6	69.2	5.8
T-83-2(	1252	54328	5.1	21.3578	3.6	0.0711	4.1	0.0110	1.8	0.44	70.6	1.3	69.7	2.7	40.1	87.2	70.6	1.3
T-83-6(	279	9839	1.3	21.3845	14.0	0.0711	14.6	0.0110	4.0	0.27	70.7	2.8	69.7	9.8	37.1	336.8	70.7	2.8
T-83-2(	224	1015	1.2	13.3602	24.5	0.0785	24.6	0.0110	2.7	0.11	70.7	1.9	76.8	18.2	270.0	568.5	70.7	1.9
T-83-1(	100	3797	1.1	16.2496	41.9	0.0939	42.3	0.0111	6.1	0.14	70.9	4.3	91.1	36.9	658.2	938.5	70.9	4.3
T-83-1(	473	13926	2.4	21.3675	4.1	0.0722	9.6	0.0112	8.7	0.90	71.8	6.2	70.8	6.6	39.1	98.1	71.8	6.2
~~T-83-3(~~	~~3192~~	~~205445~~	~~2.1~~	~~20.8552~~	~~0.8~~	~~0.0868~~	~~4.7~~	~~0.0131~~	~~4.6~~	~~0.98~~	~~84.1~~	~~3.9~~	~~84.5~~	~~3.8~~	~~36.8~~	~~19.4~~	~~84.1~~	~~3.9~~

Final Age = 68±1.0 Ma